Rates and Mechanisms of Mineral Carbonation in Peridotite: Natural Processes and Recipes for Enhanced, in situ CO_2 Capture and Storage

Peter B. Kelemen,[1] Juerg Matter,[1] Elisabeth E. Streit,[1] John F. Rudge,[2] William B. Curry,[3] and Jerzy Blusztajn[3]

[1]Lamont Doherty Earth Observatory, Columbia University, Palisades, New York 10964; email: peterk@ldeo.columbia.edu

[2]Institute of Theoretical Geophysics, Bullard Laboratories, University of Cambridge, Cambridge, CB3 0EZ, United Kingdom

[3]Woods Hole Oceanographic Institution, Woods Hole, Massachusetts 02543

Annu. Rev. Earth Planet. Sci. 2011. 39:545–76

First published online as a Review in Advance on March 1, 2011

The *Annual Review of Earth and Planetary Sciences* is online at earth.annualreviews.org

This article's doi: 10.1146/annurev-earth-092010-152509

0084-6597/11/0530-0545$20.00

Keywords

hydrothermal alteration, ophicalcite, listwanite, retrograde metamorphism

Abstract

Near-surface reaction of CO_2-bearing fluids with silicate minerals in peridotite and basalt forms solid carbonate minerals. Such processes form abundant veins and travertine deposits, particularly in association with tectonically exposed mantle peridotite. This is important in the global carbon cycle, in weathering, and in understanding physical-chemical interaction during retrograde metamorphism. Enhancing the rate of such reactions is a proposed method for geologic CO_2 storage, and perhaps for direct capture of CO_2 from near-surface fluids. We review, synthesize, and extend inferences from a variety of sources. We include data from studies on natural peridotite carbonation processes, carbonation kinetics, feedback between permeability and volume change via reaction-driven cracking, and proposed methods for enhancing the rate of natural mineral carbonation via in situ processes ("at the outcrop") rather than ex situ processes ("at the smokestack").

1. INTRODUCTION

Mineral carbonation has been proposed as a method for safe, essentially permanent CO_2 storage (e.g., Lackner et al. 1995, Seifritz 1990). The fastest mineral carbonation rates known are for the mineral olivine. Also, among abundant rock-forming minerals, olivine has the highest molar proportion of divalent cations needed to form natural carbonate minerals such as magnesite. Rocks rich in the mineral olivine are known as peridotites. In situ mineral carbonation, which involves transport of CO_2-bearing fluids into rock reactants, is distinguished from ex situ methods, which involve transport of solid reactants to a concentrated source of CO_2 such as fossil fuel–burning power plant.

In this review, we discuss research on in situ carbonation of minerals in peridotite, expand on our papers about mineral carbonation (Kelemen & Matter 2008, Matter & Kelemen 2009), and outline opportunities for future research on this subject. Much of the emphasis is on natural rates and processes, including our own research on two natural peridotite carbonation systems, one ancient and one ongoing, whose products are exposed in the peridotite of northern Oman. In addition to the intrinsic interest of these systems for earth scientists, engineers have much to learn through understanding how natural processes achieve almost 100% carbonation of peridotite. To maximize the practical utility of this review, we limit our discussion of natural processes to pressures less than 2 kbar, corresponding to depths less than ~7 km. Kinetic data indicate that olivine combines with CO_2 to form solid carbonates more rapidly than does the mineral plagioclase, the primary constituent of basalt, so we focus on peridotite. Nonetheless, we also offer some comparative information about in situ basalt carbonation.

This review has two parts: this journal article, and an electronic supplement that contains extended discussion and annotated bibliographies on many topics. The latter is available from the **Supplemental Materials link** on the Annual Reviews home page at **http://www.annualreviews.org**. The article is written to stand on its own and contains brief summaries of essential material from the supplement. However, there is little redundancy. For interested readers, a capital S preceding section, figure, and table numbers (e.g., Section S1) indicates material in the supplement. The article and supplement contain separate reference lists that are overlapping but not identical.

Mineral carbonation: reaction of silicate or oxide minerals with CO_2 in fluid to form solid carbonate minerals

Olivine: the most abundant mineral in Earth's upper mantle, $(Mg,Fe)_2SiO_4$

Magnesite: the most common magnesium carbonate mineral, $MgCO_3$, with minor Ca and Fe substitution

Peridotite: a rock composed of more than 40% olivine and less than 10% plagioclase

Plagioclase: one of the feldspar group of minerals, mainly $NaAlSi_3O_8$-$CaAl_2Si_2O_8$

Basalt: the most common form of lava on Earth, typically with 48 to 53 wt% SiO_2; when fully crystalline, common basalts are a mixture of ~60% plagioclase, 30% clinopyroxene, and 10% olivine

Quartz: a mineral composed of SiO_2

2. NATURAL PERIDOTITE CARBONATION VIA HYDROTHERMAL ALTERATION AND WEATHERING

2.1. Extent of Peridotite Near Earth's Surface

To assess the size of the geochemical reservoir represented by carbonate in natural peridotites, and the potential size of the engineered CO_2 storage reservoir, it is important to consider the mass of peridotite available at and near the surface. In the electronic supplement, **Supplemental Section S1** presents a review of this topic, and a more detailed review for the United States is provided by Krevor et al. (2009). For continuity, we provide a summary here. In considering these data, it is useful to keep in mind that average hydrothermally altered peridotite from oceanic crust contains ~0.6 wt% CO_2 in carbonate minerals, at least within 200 m of the seafloor, and that complete carbonation of 1 kg of Mg-olivine (forsterite, Mg_2SiO_4) can consume up to 0.6 kg of dissolved CO_2 from fluid to produce 1.6 kg of magnesite ($MgCO_3$) and quartz (SiO_2).

In the upper 7 km of the solid Earth, peridotite is generally found in five settings, listed in order of decreasing abundance:

1. In oceanic crust and shallow mantle, especially in oceanic crust formed at slow-spreading mid-ocean ridges where 5 to 15% of the newly formed seafloor is underlain by altered, mantle peridotite (Cannat et al. 1995, Carlson 2001)

Supplemental Material

2. In the forearc regions of subduction-related magmatic arcs
3. In subaerial massifs known as ophiolites, which are thrust sheets of mafic crust and shallow mantle formed at submarine spreading ridges and then thrust over continental crust via plate tectonic processes
4. In large, mafic to ultramafic, igneous intrusions
5. In peridotite massifs where tectonic processes, typically including crustal extension, have exposed the ancient, continental upper mantle

Ophiolite: a thrust sheet of crust and upper mantle formed at an oceanic spreading ridge and then emplaced onto a continental margin via plate tectonic collisions

Slow-spreading mid-ocean ridges emplace 1–4 $\times$ 10^{12} kg year^{-1} of peridotite in the upper 7 km of the oceanic plates, or $\sim 10^{18}$ kg of peridotite in a swath 10 km wide on either side of the slow-spreading ridges over 1 Ma. Peridotite extends beneath a shallow veneer of pelagic sediment for thousands of kilometers on either side of the slow-spreading Mid-Atlantic and Indian Ocean Ridges, corresponding to more than 10^{20} kg of material. There is no quantitative estimate of the proportion of peridotite in forearc settings, but its total mass is probably larger than the mass of peridotites in ophiolites. The Samail ophiolite, in the Sultanate of Oman and the United Arab Emirates, contains approximately 5 $\times$ 10^{16} kg of peridotite within 3 km of the surface (Kelemen & Matter 2008). Peridotite in ophiolites is found on all continents, with a total mass between 10^{17} and 10^{18} kg. The gigantic, igneous Bushveld layered intrusion in South Africa contains 10^{16} to 10^{17} kg of peridotite and pyroxenite, and the similar Stillwater intrusion in Montana contains almost 10^{15} kg of peridotite. Continental peridotite massifs may have a combined mass on the order of 10^{15} kg.

2.2. Simplified Metamorphic Reactions for Peridotite Carbonation

Peridotite is a rock type composed of >40% of the mineral olivine (with the gemstone name peridot). Typical residual mantle peridotite exposed on the seafloor and in ophiolites is composed of 70–85% olivine. Bands of dunite are present within the peridotite and comprise 5–15% of the mantle section in many ophiolites. Dunite contains more than 95% olivine. Carbonation of the mineral olivine occurs together with hydration via the simplified reactions

$$4Mg_2SiO_4(\text{Mg-olivine}) + 4H_2O + 2CO_2 = 2Mg_3Si_2O_5(OH)_4(\text{serpentine}) + 2MgCO_3(\text{magnesite}), \quad (1a)$$

$$4Mg_2SiO_4 + H_2O + 5CO_2 = Mg_3Si_4O_{10}(OH)_2(\text{talc}) + 5MgCO_3, \text{ and} \quad (1b)$$

$$4Mg_2SiO_4 + 8CO_2 = 4SiO_2(\text{quartz}) + 8MgCO_3. \quad (1c)$$

After hydration, carbonation occurs via the simplified reactions

$$4Mg_2SiO_4 + 6H_2O = 2Mg_3Si_2O_5(OH)_4 + 2Mg(OH)_2(\text{brucite}), \quad (1d)$$

$$\text{products of 1d} + 2CO_2 = 2Mg_3Si_2O_5(OH)_4 + 2MgCO_3 + 2H_2O, \quad (1e)$$

$$\text{products of 1e} + 3CO_2 = Mg_3Si_4O_{10}(OH)_2 + 5MgCO_3 + 5H_2O, \text{ and} \quad (1f)$$

$$\text{products of 1f} + 3CO_2 = 4SiO_2 + 8MgCO_3 + 6H_2O. \quad (1g)$$

These reactions are written with no components other than H_2O and CO_2 in fluids, but of course they can take on infinite variety when other key components—such as Ca^{2+}, aqueous SiO_2, H_2, sulfur species, and O_2—are considered to be transported in fluids.

Pyroxene: the second most abundant group of minerals in Earth's shallow mantle, containing mainly $(Mg,Fe,Ca)_2Si_2O_6$

Ca-poor pyroxene: pyroxene rich in $(Mg,Fe)_2Si_2O_6$, known as orthopyroxene or opx

Ca-rich pyroxene: pyroxene composed mainly of $(Mg,Fe)CaSi_2O_6$, known as clinopyroxene or cpx

Serpentine: a hydrous alteration product of olivine, mainly $(Mg,Fe)_3Si_2O_5(OH)_4$

Talc: a hydrous magnesium silicate, $(Mg,Fe)_3Si_4O_{10}(OH)_2$

Dolomite: the most common calcium-magnesium carbonate mineral, $CaMg(CO_3)_2$, with minor Fe substitution

Calcite: the most common calcium carbonate mineral, $CaCO_3$, with minor Mg and Fe substitution

Goethite: a hydrous ferric iron mineral, FeO(OH)

Brucite: magnesium hydroxide, $Mg(OH)_2$, sometimes with important Fe substitution

Hematite: a ferric iron oxide mineral, Fe_2O_3

Magnetite: an iron oxide mineral with mixed Fe valence, Fe_3O_4

The second and third most abundant minerals in peridotite are Ca-poor pyroxene (often termed orthopyroxene or opx, with Mg-end-member enstatite, $Mg_2Si_2O_6$) and Ca-rich pyroxene (often termed clinopyroxene or cpx, with Mg-end-member diopside, $CaMgSi_2O_6$). To understand natural peridotite carbonation, it is important to add the simplified reaction:

$$4Mg_2SiO_4 + CaMgSi_2O_6 + 6H_2O + CO_2 = 3Mg_3Si_2O_5(OH)_4 + CaCO_3(\text{calcite}). \quad (1h)$$

This reaction often takes place in stages; that is,

$$4Mg_2SiO_4 + CaMgSi_2O_6 + 7H_2O = 3Mg_3Si_2O_5(OH)_4 + Ca^{2+}(aq) + 2OH^-(aq) \quad (1i)$$

occurs in the subsurface, and then

$$Ca^{2+}(aq) + 2OH^-(aq) + CO_2(\text{aq or gas}) = CaCO_3 + H_2O \quad (1j)$$

occurs when fluids modified by reaction with peridotite form travertine at or near the surface.

Mantle peridotite generally has molar Mg/(Mg + Fe), or Mg#, of ~0.9. Iron is dissolved in silicates (e.g., $Mg_{1.8}Fe_{0.2}SiO_4$ olivine) and oxides. During hydration and carbonation, reaction products such as serpentine, talc, magnesite, dolomite, and calcite have higher Mg# values than do the olivine and pyroxene reactants (Beard et al. 2009, Evans 2008, Frost 1985, Frost & Beard 2007, Horita & Berndt 1999, Janecky & Seyfried 1986, Klein et al. 2009; Klein & Bach 2009, McCollom & Bach 2009). Excess iron is commonly taken up by hydroxides such as goethite [FeO(OH)] and brucite [$(Mg,Fe)(OH)_2$], by oxides such as hematite (Fe_2O_3) and magnetite (Fe_3O_4), and by metal alloys rich in Fe and Ni such as awaruite, as observed in Oman (Lorand 1987). Initial stages of reaction in rock-dominated systems often involve oxidation of iron from Fe^{2+} in silicates such as olivine to Fe^{3+} in oxides. These and other reactions lead to reduced oxygen fugacity and increased hydrogen fugacity in product fluids, e.g.,

$$6Fe_2^{2+}SiO_4 + 7H_2O = 3Fe_3^{2+}Si_2O_5(OH)_4(\text{Fe} - \text{serpentine}) + Fe_2^{3+}Fe^{2+}O_4(\text{magnetite}) + H_2(aq). \quad (1k)$$

In this way, fluids become increasingly reduced as the fluid/rock ratio decreases and eventually saturate in Fe-Ni alloys. Fluids from serpentinizing peridotites have low oxygen fugacity and enhanced levels of dissolved hydrogen and methane (Barnes & O'Neil 1969; Haggerty 1991, Kelley et al. 2005, Lang et al. 2010, Peretti et al. 1992), as observed in Oman (e.g., Neal & Stanger 1983). From the perspective of mineral carbonation, the main impacts of these redox reactions are to impart a geochemical signal (low oxygen fugacity, high fugacity of H_2) to fluids produced by hydration of peridotite at low water/rock ratios and to impart the potential for reduction of carbon species, including breakdown of carbonate minerals to form graphite and methane, e.g.,

$$MgCO_3 + 2H_2 = Mg(OH)_2(\text{or aqueous } Mg^{2+} + 2OH^-) + H_2O + C(\text{graphite}) \quad (1l)$$

and

$$MgCO_3 + 4H_2 = Mg(OH)_2 + H_2O + CH_4(\text{methane}). \quad (1m)$$

The reactions listed here and their associated mineral parageneses were explored decades ago (e.g., Evans 1977; Frost 1985; Greenwood 1967; Johannes 1969; Kerrick 1974; Skippen 1974; Trommsdorff & Evans 1977a,b). As noted by these previous workers, peridotite carbonation reactions progressively form increasingly SiO_2-rich silicates, as Mg and Ca are incorporated into carbonate minerals with increasing CO_2 contents in fluid at a given pressure and temperature (**Figure 1**). In the absence of H_2O-rich fluids, the maximum thermal stability of carbonate minerals in peridotite bulk compositions at 2 kbar are approximately 520°C for breakdown of magnesite + quartz to form opx + CO_2, and 560°C for breakdown of magnesite + opx to form olivine + CO_2 (Johannes 1969). At lower P_{CO_2}, in the presence of aqueous fluids and/or at lower total pressure, the thermal stability of carbonate minerals is reduced.

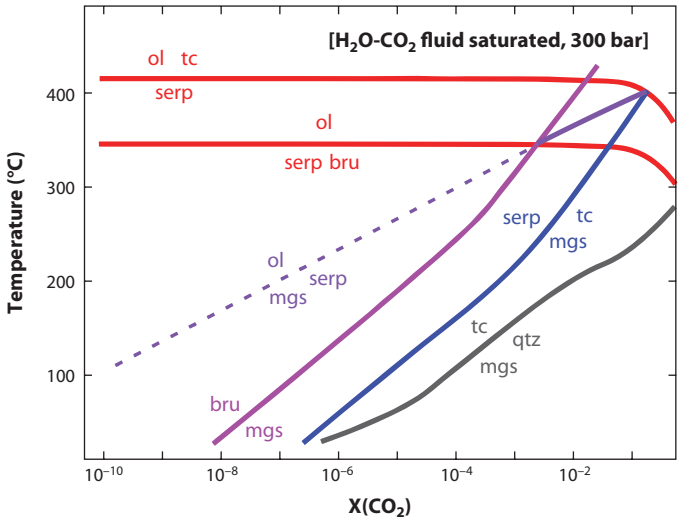

Figure 1

Schematic phase diagram for reactions involving brucite (bru), olivine (ol), the serpentine polymorph chrysotile (serp), talc (tc), quartz (qtz), and magnesite (mgs) in the system $MgO\text{-}SiO_2\text{-}H_2O\text{-}CO_2$, saturated in $H_2O\text{-}CO_2$ fluid at 300 bar, calculated using Thermocalc (Holland & Powell 1998).

2.3. Aqueous Geochemistry of Peridotite Carbonation

As originally explained by Barnes, O'Neil, and coworkers (Barnes & O'Neil 1969; Barnes et al. 1967, 1978) and quantified by Bruni, Cipolli, Marini and coworkers (Bruni et al. 2002, Cipolli et al. 2004), low-temperature reaction between surface waters and peridotite generally takes place in three steps. First, meteoric water reacts with peridotite in equilibrium with the atmosphere, increasing dissolved Mg^{++} and HCO_3^- concentrations to form Mg-HCO_3 waters, also known as Type I waters. Type I waters are found in shallow groundwater in peridotite massifs worldwide.

In the second step, subsurface reaction, out of equilibrium with the atmosphere, leads to precipitation of Mg-carbonates such as magnesite and dolomite, together with serpentine and clay minerals. Although Ca is a minor constituent of the peridotite, contained mainly in pyroxene minerals, it is excluded almost completely from serpentine and clay, and the concentration of Ca^{++} in resulting fluids rises even when dolomite—$CaMg(CO_3)_2$—is precipitating. Dissolution of Ca-bearing pyroxenes also leads to very high pH, as in Reaction 1i above, whereas reactions such as Reaction 1k reduce the oxygen fugacity to very low values (e.g., Barnes & O'Neil 1969, Bruni et al. 2002, Cipolli et al. 2004, Evans 2008, Frost 1985, Janecky & Seyfried 1986). Carbonate precipitation via Reactions 1a–g, together with reactions such as

$$Mg^{++} + HCO_3^- + OH^- = MgCO_3 + H_2O, \quad (2)$$

lowers the total carbon concentration in the resulting fluids to nearly zero (Barnes & O'Neil 1969, Bruni et al. 2002, Cipolli et al. 2004), producing high-pH, low-fO_2, low-carbon Ca-OH waters, sometimes termed Type II waters. These form alkaline springs that emerge from peridotite catchments worldwide.

In the third step, alkaline spring waters react with the atmosphere (or mix with shallow groundwater), precipitating calcite and lowering the pH to neutral values via reactions such as Reaction 1j.

Awaruite: an Fe-Ni alloy mineral

Paragenesis: common assemblage of rock-forming minerals, often indicative of crystallization at a particular pressure, temperature, and/or fluid composition

2.4. Observed Parageneses on Land, Especially in the Samail Ophiolite in Oman

Ophicalcite: carbonate-rich, hydrothermally altered peridotite

Listwanite (also spelled listvenite, listvanite, listwaenite): completely carbonated peridotite, with all Mg and Ca and some Fe in carbonate minerals, and all SiO_2 in quartz

Serpentinite: a rock composed almost entirely of the mineral serpentine

Supplemental Material

Peridotite-hosted carbonates come in essentially three types: (*a*) partially hydrated peridotite with carbonate veins, sometimes termed ophicalcite, especially in Alpine localities, (*b*) fully carbonated peridotite (magnesite or dolomite + quartz) known as listwanite (also known as listvenite, listvanite, or listwaenite), and (*c*) travertine deposited from springs in peridotite catchments. In **Supplemental Section S2**, we provide an annotated bibliography of work on these parageneses in subaerial outcrops worldwide. Here we focus on outcrops in Oman.

The Samail ophiolite in northern Oman and the eastern United Arab Emirates has been the site of classic studies of hydrothermal alteration of lower crust and upper mantle formed at an oceanic spreading ridge (e.g., Bosch et al. 2004, Gregory & Taylor 1981). Boudier et al. (2010) recently made detailed investigations of serpentinite replacement textures, and two short papers report on native metal alloys in Oman serpentinites (Leblanc et al. 1991, Lorand 1987). Dewandel et al. (2003, 2005), Weyhenmeyer et al. (2002), and Matter et al. (2006) studied the hydrology of parts of the ophiolite and peridotite alluvium.

Peridotites in Oman are generally 30–70% serpentinized, although 100% hydrated rocks (serpentinites) are found, particularly in large areas with low relief. The proportion of serpentine formed during hydrothermal circulation near a spreading ridge, versus the proportion formed during obduction versus the proportion formed during weathering, is not known. However, the qualitative observation that peridotites appear to be fresher in deep canyons than in low relief areas suggests that much of the serpentinization formed during ongoing, subaerial weathering and that its extent decreases with depth below the surface (A. Nicolas and F. Boudier, personal communication, 1990). Submillimeter-wide carbonate veins are found on almost all joint surfaces in new roadcuts, and massive magnesite veins can be seen traversing the peridotite landscape. Extensive, spectacular travertine deposits form around alkaline springs in peridotite catchments. Veins are generally composed of magnesite and/or dolomite far from travertines, and calcite and/or dolomite directly beneath travertines.

The ophiolite contains both listwanite and "normal," partially serpentinized, peridotite-hosting carbonate veins. On the basis of data in Section 2.7 and in **Supplemental Section S4**, we conclude that most of the carbonate veins form in currently active low-temperature systems—at 30°C to perhaps 60°C—that involve meteoric water. In contrast, listwanites formed in fossil high-temperature systems that reached ~200°C. Stanger and coworkers (Stanger 1985, 1986; Stanger & Neal 1994; Stanger et al. 1988) wrote several papers on the present-day peridotite alteration and seminal papers on groundwater and alkaline springs formed by peridotite alteration (Neal & Stanger 1983, 1984, 1985). Clark and coworkers (Clark & Fontes 1990, Clark et al. 1992) studied a peridotite-hosted travertine, mainly in an effort to obtain a stable isotope record of paleoclimate. There have been several studies of listwanites in Oman (Nasir et al. 2007, Stanger 1985, Wilde et al. 2002).

New ^{14}C "ages" for all but two of 44 peridotite-hosted travertine and carbonate vein samples from the low-temperature system are <50,000 years old (our unpublished data and Kelemen & Matter 2008). This suggests that low-temperature peridotite alteration is close to a steady state in which carbonates form in a shallow weathering horizon at approximately the same rate that this horizon is removed by erosion. In our view, there is little indication that paleoclimatic variation is recorded by stable isotope ratios in peridotite-hosted carbonates (**Supplemental Section S3**). In the subsurface, with increasing solid volume, one might expect decreasing permeability and armoring of reactive surfaces to limit the extent of reaction, yet the ^{14}C data indicate that low-temperature alkaline springs feeding travertine deposits remain active for tens of thousands of years.

Assuming that the rate of carbonate formation has been approximately constant for 50,000 years, we infer that $\sim 5 \times 10^4$ tons of peridotite-hosted carbonate form per year in Oman (**Supplemental Tables S1** and **S2**; also see Kelemen & Matter 2008). Information on the constraints and uncertainties in this rate estimate is given in **Supplemental Section S4**.

Travertine terraces form by low-temperature reaction of dissolved Ca with atmospheric CO_2, as in Reaction 1j, where alkaline spring waters exit from peridotite. Groundwater (Type I, Mg-HCO_3 waters) and alkaline spring water (Type II, Ca-OH waters) conform well to the compositional groups and hypotheses outlined by Barnes & O'Neil (1969) and Bruni et al. (2002). As noted in the previous section, Type I waters have high total carbon, whereas the most alkaline Type II waters have almost none, indicative of subsurface Ca-Mg carbonate precipitation. Carbonate veins in partially serpentinized peridotite have ^{14}C ages that overlap the travertine ages, and stable isotope data yield crystallization temperatures of 20–60°C for both veins and travertines, so the veins probably represent the subsurface carbonate complementary to Type II waters and travertine deposition (**Supplemental Section S4** and Kelemen & Matter 2008). Metamorphic parageneses in veined peridotites also show that they formed at <50°C, near the surface (E. Streit, P. Kelemen & J. Eiler, unpublished data).

Extensive listwanites in the Oman peridotites—billions of tons of fully carbonated peridotite—are inferred to be late Cretaceous or Paleocene on the basis of one locality in which they replace mantle peridotite, which was thrust onto the Arabian continent beginning at ~96 Mya (e.g., Hacker 1994). Additionally, the listwanites are unconformably overlain by late Paleocene to Eocene conglomerate and limestone (23.44°N, 56.19°E). Preliminary stable isotope data (E. Streit, P. Kelemen & J. Eiler, unpublished data) suggest that they formed at a peak temperature of ~200°C, similar to that of listwanites elsewhere (Hansen et al. 2005, Madu et al. 1990, Schandl & Naldrett 1992, Schandl & Wicks 1991). If so, they probably formed from fluids rich in CO_2 because magnesite + quartz are not stable, and they probably break down to form talc + CO_2 in the presence of H_2O-rich fluids at 200°C (**Figure 2**). All known listwanites in Oman are found within 500 m of the basal thrust, where peridotites overlie CO_2-bearing metasediments. It is likely that CO_2-rich fluids, formed by metamorphic dehydration of the underlying sediments as they were overthrust by hot peridotite, rose into the peridotite to form the listwanites.

2.5. Observed Parageneses on the Seafloor

Formation of carbonate via reaction of fluid with peridotite is occurring at and beneath the seafloor flanking slow-spreading mid-ocean ridges via submarine "weathering" as well as in more spectacular hydrothermal vent systems. In both settings, peridotite carbonation is inextricably linked with hydration. An annotated bibliography of work on these sites, and related work on phase equilibrium in these systems, is given in **Supplemental Section S5**.

Serpentine-rich mud volcanoes and associated carbonate chimneys in forearc settings attest to the importance of hydrothermal interaction with peridotite in the mantle wedge above subduction zones (Eickmann et al. 2009; Haggerty 1991; Mottl et al. 2003, 2004). This important setting for peridotite carbonation has not received sufficient attention. The Oman listwanites, formed in peridotite thrust over carbonate-bearing sediments, provide an outcrop exposure of peridotite carbonation processes in the hanging wall of a subduction zone.

Subseafloor peridotite carbonation is most spectacularly evident at the tall carbonate chimneys of the Lost City hydrothermal area, ~15 km west of the Mid-Atlantic Ridge at 30°N (e.g., Früh-Green et al. 2003, Kelley et al. 2001, Ludwig et al. 2006). High-pH (~11) and low-Eh vent fluids are similar to Type II waters in alkaline springs on land. Exit fluid temperatures at Lost City are 40–75°C, higher than in subaerial Type II springs but much lower than maximum fluid

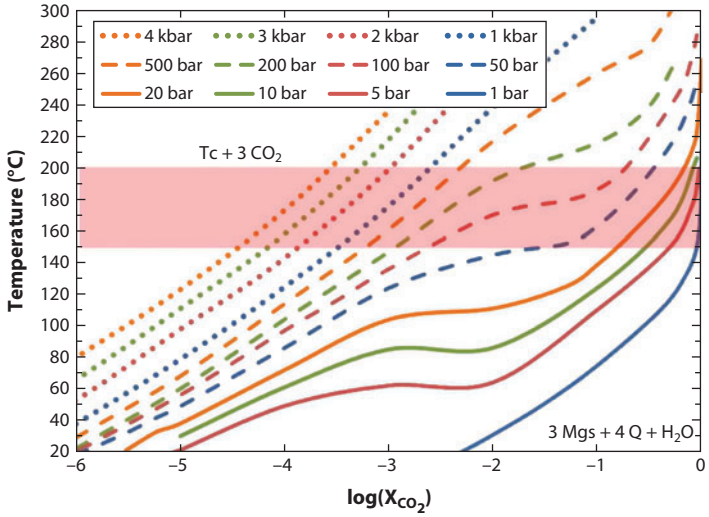

Figure 2

Mole fraction of CO_2 in H_2O-CO_2 fluid X_{CO_2} versus temperature, for the reaction talc (Tc) + CO_2 = magnesite (Mgs) + quartz (Q) + H_2O, calculated for Mg-end-members using Thermocalc (Holland & Powell 1998). At a given pressure, the assemblage magnesite + quartz at high temperature is stable only in the presence of CO_2-rich fluids. The shaded band shows the likely temperature of formation of Oman listwanites. The pressure of listwanite formation is not well constrained but was probably less than 4 kbar.

temperatures at other hydrothermal vent sites along mid-ocean ridges. An even lower-temperature (maximum 40°C), peridotite-hosted, alkaline spring forming a carbonate chimney is known just offshore from New Caledonia (Launay & Fontes 1985).

Kelley et al. (2001) suggested that, whereas other vent sites have a magmatic heat source, Lost City may be heated by exothermic hydration of peridotite (serpentinization), as proposed in general by Schuiling (1964) and Fyfe (1974). Exothermic heating via peridotite carbonation may also be important (Kelemen & Matter 2008). Experimental data coupled with thermodynamic calculations (Allen & Seyfried 2004, Seyfried et al. 2007) suggest that maximum fluid temperatures in the subsurface may have been ~200°C, with subsequent cooling to produce 40–75°C exit fluids at Lost City. Conductively cooled, diffusely venting fluids around other, higher-temperature, peridotite-hosted vent sites reach solid carbonate saturation, as in carbonate-cemented breccias around the Rainbow and Saldanha vent sites (Ribeiro Da Costa et al. 2008).

In general, diffuse interaction between seafloor peridotite and seawater at low temperature probably produces more solid carbonate than do the more spectacular features at focused hydrothermal vents, as discussed in **Supplemental Section S5**. **Figure 3** illustrates the observed concentration of CO_2 in drill holes from Ocean Drilling Program (ODP) Legs 153 and 209, at ~23°N and 15°N along the Mid-Atlantic Ridge, as a function of depth below the seafloor, extending to approximately 200 meters below seafloor (mbsf) (Casey 1997, Kelemen et al. 2004). These peridotites contain an average of 0.6 wt% CO_2 in carbonate minerals, without systematic variation with depth. Some seafloor peridotites may also contain graphite (Berndt et al. 1996).

2.6. Global Significance of Natural Peridotite Carbonation

In this section, we assess the amount of carbon in near-surface peridotite compared with the amount of carbon in the hydrosphere. There may be several sources of carbon involved.

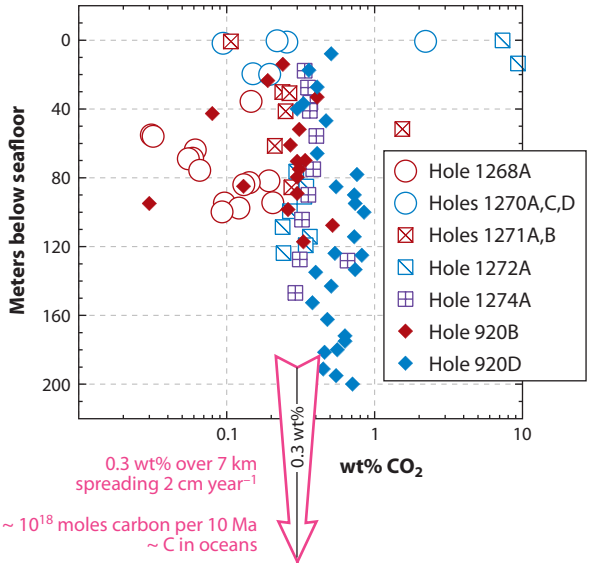

Figure 3

Concentration of carbon (expressed as wt% CO_2, although some could be in the form of graphite) versus depth (meters below seafloor) in peridotite drill core recovered on Ocean Drilling Program (ODP) Legs 153 and 209 (Casey 1997, Kelemen et al. 2004). There is no systematic variation of carbon concentration with depth, and the average concentration is 0.6 wt% CO_2. (See also Früh-Green et al. 2004, figure 8.) As described in the text, where peridotite is exposed on the seafloor at slow-spreading ridges, oceanic crust may have an average carbon concentration expressed as 0.3 wt% CO_2 extending to 7-km depth, as illustrated schematically by the pink arrow. If so, this corresponds to uptake of 10^{18} moles of carbon every 10 Ma, equivalent to the amount of carbon dissolved in the ocean.

1. The budget is dominated by carbon uptake from seawater and groundwater during hydrothermal alteration and weathering.
2. Uptake of carbon from magmatic fluids, where mafic plutons are emplaced into mantle peridotite (along slow-spreading ridges and perhaps in some subduction-related arcs), may form carbonate minerals.
3. There may be "primary" carbon in mantle peridotites, which could be preserved where uplift and erosion that expose peridotite on the surface are very slow, in regions with low heat flow.

(2) and (3) are small by comparison with (1), and are discussed in **Supplemental Section S6**.

As noted above, drill-core samples of peridotite from the Mid-Atlantic Ridge have an average CO_2 concentration of 0.6 wt% (**Figure 3**). In the 15°N area along the Mid-Atlantic Ridge, peridotite intruded by gabbroic plutons is regionally extensive on both sides of the spreading axis. Seismic data for this area suggest that gradually decreasing proportions of serpentinization extend to 6–8 km below the seafloor (figure F5 in Kelemen et al. 2004). Where peridotite is exposed on the seafloor flanking slow-spreading ridges [5–15% of the total area (Cannat et al. 1995, Carlson 2001)], assuming that the serpentinization gradient is linear and associated with carbonation, there may be ~0.3 wt% CO_2 over a 7-km depth interval. Then, for an average half-spreading rate of 0.01 m per year over a length of 60,000 km, peridotite alteration around slow-spreading ridges consumes $\sim 10^{11}$ moles of carbon per year, or $\sim 2 \times 10^6$ moles per kilometer per year. This is roughly one-tenth of the global uptake via alteration of basaltic lavas on the seafloor at fast- and slow-spreading ridges combined (Alt & Teagle 1999, Staudigel & Hart 1985). Peridotite

carbonation during 10 Ma of spreading consumes $\sim 10^{18}$ moles of carbon, equivalent to the mass of carbon in the oceans. Extrapolating the estimated rate of CO_2 uptake by peridotite carbonation in Oman—5×10^4 tons per year or $\sim 10^7$ moles per kilometer per year over the 350-km length of the Samail ophiolite—to ophiolites worldwide yields $\sim 5 \times 10^9$ moles of carbon per year, which is small in comparison with peridotite carbonation beneath the seafloor.

Peridotite carbonation may be an ongoing process that continues far off axis, by analogy with carbonate formation in basaltic lavas formed at mid-ocean ridges that continues for at least 150 Ma despite their gradual burial beneath pelagic sediments (Alt & Teagle 1999, Staudigel & Hart 1985). If the carbonation process continues for hundreds of kilometers off axis, CO_2 contents in peridotites from ODP Legs 153 and 209 (close to the Mid-Atlantic Ridge) may be lower than those beneath sediments further off axis, and the total rate of CO_2 consumption via peridotite carbonation would be correspondingly higher.

Supplemental Material

2.7. Stable Isotope Data: Mineral Crystallization Thermometry

We collected preliminary, whole-rock data on oxygen and carbon isotopes in peridotite-hosted travertine and vein samples from Oman (**Figure 4** and **Supplemental Table S3**). These show two important features: (*a*) kinetic fractionation of both carbon and oxygen isotopes in travertine samples less than 1,000 years old, and (*b*) apparent equilibrium of older travertines with groundwater and spring water, recording near-surface temperatures. The kinetic fractionation seen in the young travertines (**Supplemental Section S7**) is of great interest but is tangential to the main topics of this review.

Some of our samples of calcite (travertine) and magnesite (veins) are pure enough that the oxygen isotope ratio for the whole rock is a close approximation of the ratio in the minerals.

Figure 4

Whole-rock carbon and oxygen isotope data on peridotite-hosted carbonate veins, and surficial travertine deposits associated with alkaline springs in peridotite catchments, in the ophiolite massifs of northern Oman. ^{14}C ages are in radiocarbon years before 1950. For our new data (**Supplemental Table S3**), error bars for ^{14}C ages are shown only for samples with replicate analyses because analytical precision for other samples is not an adequate reflection of the intrasample variability within our samples. (*a*) Our new data (*filled symbols*) and those of Clark & Fontes (1990; *open symbols*). For the data of Clark & Fontes (1990), analytical precision and data on replicate analyses are not given for stable isotope data, but precision is listed (and shown) for ^{14}C ages. (*b*) In addition to data from Oman (*diamonds*, as in panel *a*), outlined fields represent data from peridotite-hosted carbonate deposits in northern California (*red* and *blue*; see below), Egypt (*green*; Smith et al. 2004), the Balkans (*purple*; Fallick et al. 1991), and northwest Canada (*orange*; Wilson et al. 2009). Blue outline: "scums," "sludges," and travertines associated with Ca-OH-type alkaline springs (O'Neil & Barnes 1971); red with gray background: Ca-Mg carbonate veins (O'Neil & Barnes 1971); dashed red: hydromagnesite veins (O'Neil & Barnes 1971); filled red rectangle: magnesite veins (Barnes et al. 1973). $\delta^{18}O$ data ranging from ~20 to 25.5 are also available for travertine from the Del Puerto ophiolite (Blank et al. 2009, not shown). (*c*) In addition to data from Oman (*diamonds*, as in panel *a*), light-green rectangles show the range of data for carbonate chimneys (LCC) and calcite veins in surrounding host rocks (LCV) from the Lost City hydrothermal area along the Mid-Atlantic Ridge (Früh-Green et al. 2003). Light-green circles and oval represent calcite in veins and ophicarbonates drilled from the Iberian Margin continent-ocean transition; compositions of 36 out of 38 samples lie in oval with bold outline (Agrinier et al. 1988, 1996; Evans & Baltuck 1988; Milliken & Morgan 1996). Yellow rectangle containing black dots: aragonite in serpentinized peridotites dredged from the Mid-Atlantic Ridge (Bonatti et al. 1980). Black dashed rectangle: calcite in Ligurian and Appenine ophicalcite deposits, ranging from lower (heavy $\delta^{18}O$) to higher metamorphic grade (light $\delta^{18}O$; Barbieri et al. 1979). White rectangles containing diagonal black lines: (*right*) calcite in oceanic ophicarbonates affected by later Alpine regional metamorphism (Früh-Green et al. 1990); (*left*) calcite in contact-metamorphosed ophicarbonates in the Bergell aureole, Val Malenco (Abart & Pozzorini 2000, Pozzorini & Früh-Green 1996). (*d*) Oxygen isotope values versus ^{14}C ages for our data (*filled symbols*) and those of Clark & Fontes (1990) (*open symbols*, as in panel *a*), illustrating that light ratios are found only in samples that are less than a few thousand years old, and that pure calcite and pure magnesite samples record low, near-surface temperatures of equilibration with Oman groundwater and spring water. Abbreviations: SMOW, per mil deviation relative to standard mean ocean water; VPDB, per mil deviation relative to Vienna Pee Dee Belemnite.

For calcite-rich travertine with ^{14}C ages of >1,000 years and carbonate veins composed mainly of calcite, typical $\delta^{18}O$ is 23–26‰ relative to SMOW (per mil deviation relative to standard mean ocean water; see bold type in **Supplemental Table S3**). If calcite formed in equilibrium with typical Oman groundwaters and alkaline spring waters having $\delta^{18}O$ from −2‰ to 1‰ (our unpublished data and Clark et al. 1992, Matter et al. 2006 , Neal & Stanger 1985), they would record ^{16}O-^{18}O exchange at ~23–60°C (Chacko & Deines 2008, Friedman & O'Neil 1977, O'Neil et al. 1969), approximately equivalent to the seasonal range of air temperature in Oman.

All but two veins (from near the oasis of Tuf) show systematically heavier $\delta^{18}O$ and $\delta^{13}C$ compared with that of travertine. We tentatively attribute this variability to variable proportions of carbonate and silicate minerals, all close to equilibrium with relatively similar fluid compositions. Two nearly pure magnesite veins have $\delta^{18}O$ of 35‰ to 36‰, yielding magnesite-water oxygen exchange temperatures of ~33°C to 49°C (Chacko & Deines 2008). Less precise data for a third magnesite-rich vein yield $\delta^{18}O$ of 30‰, corresponding to 58–74°C. Of three veins with more than 60 wt% dolomite, two have $\delta^{18}O$ between 31‰ and 32‰. If these approximate the oxygen isotope

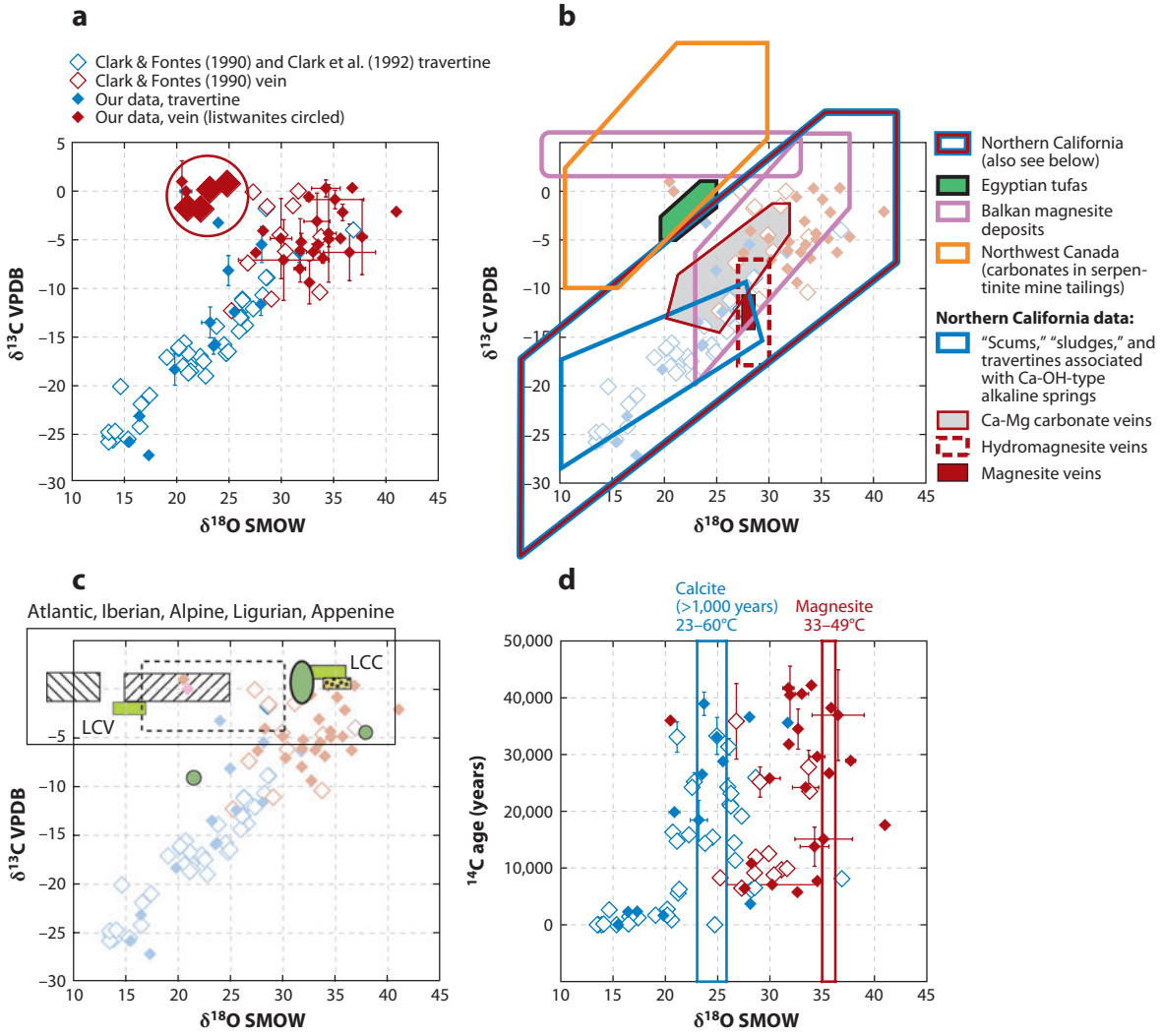

ratio in dolomite, they yield low crystallization temperatures (Tarutani et al. 1969, Vasconcelos et al. 2005) consistent with the temperatures calculated for calcite and magnesite. A third dolomite-rich sample with $\delta^{18}O$ ~41 yields an unreasonably low temperature.

The temperatures calculated here, for stable isotope exchange between peridotite-hosted carbonates and groundwater in Oman, are consistent with observed temperatures of alkaline spring waters and with temperatures of hydrogen isotope fractionation between gas and alkaline spring waters in Oman (Neal & Stanger 1983). Similarly, in the California Coast Ranges (Barnes et al. 1973, Blank et al. 2009), calcite- and dolomite-bearing travertines with $\delta^{18}O$ of 20–25‰ and magnesite veins with $\delta^{18}O$ of 27.6–28.2‰ record equilibrium with local waters at 15–40°C. All these data suggest that magnesite veins in partially carbonated peridotites and alkaline spring waters are genetically related and that they form via fluid-rock reaction at approximately the same temperature as travertine, near the surface in a shallow weathering horizon, as hypothesized by Kelemen & Matter (2008).

Supplemental Section S8 summarizes data on stable isotopes in peridotite-hosted carbonates from seafloor samples and the Alps. Unlike samples from Oman, California, Canada, and the Balkans, the Swiss and northern Italian samples have restricted $\delta^{13}C$ from approximately −4‰ to 3‰. Furthermore, they show a range of $\delta^{18}O$ that corresponds to expected depositional and metamorphic temperatures, from near 0°C for samples formed near the seafloor to more than 100°C in Alpine metamorphic rocks.

It is important to constrain the conditions of listwanite formation because complete carbonation is the goal of enhanced peridotite carbonation for CO_2 capture and storage. So far, most of our stable isotope data on Oman samples are for travertines and carbonate veins from serpentinized peridotite, not from listwanites. Furthermore, we do not know $\delta^{18}O$ in the fluids that formed listwanites. If we assume that $\delta^{18}O$ was near zero, as in Type I and II waters in Oman peridotites today, preliminary oxygen isotope data yield formation temperatures of 40–70°C for calcite and 100–150°C for magnesite. However, this assumption is highly questionable for Cretaceous, metamorphic fluids that could have been derived from isotopically heavy metasediments.

Consistent listwanite formation temperatures of 237 ± 21°C, 248 ± 12°C, and 210–240°C were determined for three localities in Canada via fluid-inclusion measurements (Hansen et al. 2005, Madu et al. 1990, Schandl & Wicks 1991). Preliminary data using the "clumped isotope" technique (Eiler 2007, Ghosh et al. 2006) show that Oman listwanites also record peak temperatures close to 200°C (E. Streit, P. Kelemen & J. Eiler, unpublished data). Inferred listwanite formation temperatures correspond well to inferred temperatures in the reaction zone beneath the Lost City hydrothermal vents (Allen & Seyfried 2004, Seyfried et al. 2007).

3. CHEMICAL KINETICS OF MINERAL CARBONATION

3.1. Experimental Dissolution and Carbonation Kinetics of Olivine, Serpentine, Plagioclase, and Basalt

In this section, we review data on the rates of dissolution and carbonation of olivine, plagioclase, and basalt, expanding on the summary by Matter & Kelemen (2009). Dissolution and carbonation of other minerals, particularly wollastonite ($CaSiO_3$) and serpentine, have been investigated in the context of CO_2 capture and storage. However, serpentine carbonation—without expensive heat treatment to ~600°C prior to reaction—is more than 10 times slower than olivine carbonation (e.g., Gerdemann et al. 2007, O'Connor et al. 2004), and wollastonite is not a common mineral.

Supplemental Section S9 provides an annotated bibliography of experimental work. For continuity, we summarize the main points here. The fastest-known olivine carbonation was observed

in unconventional studies at the U.S. Department of Energy's Albany Research Center and at Arizona State University. These studies combined olivine dissolution with carbonate precipitation, at an olivine-to-water ratio of ~1:4. Olivine in saline aqueous solutions with high bicarbonate (e.g., $NaHCO_3$, $KHCO_3$) concentrations were held in a closed reaction vessel at high P_{CO_2} (e.g., Chizmeshya et al. 2007, O'Connor et al. 2004). The fastest rates were at 185°C in aqueous solutions with 1 M NaCl and 0.64 M $NaHCO_3$ with $P_{CO_2} > 70$ bar and pH ~ 8. At high P_{CO_2}, high bicarbonate concentrations act as a catalyst, making rates 1,000 times faster than rates for the same conditions without bicarbonate and more than 10^6 times faster than rates observed and calculated at 25°C, at pH 8, and with atmospheric P_{CO_2} (**Figure 5**). Experimental olivine carbonation, together with carbonation of basaltic glass (inferred from dissolution rate data), is much faster than dissolution of basalt or minerals common in basaltic rocks.

Importantly, it seems that there are no experiments on dissolution of plagioclase or basalt with high $NaHCO_3$. If high-$NaHCO_3$ solutions catalyze rapid basalt carbonation, comparable with the effect for olivine, then basalt carbonation would be a favorable mineral carbonation method because basalt is the most common rock type in Earth's crust.

Extrapolation of chemical kinetic data on powders to natural peridotite carbonation requires knowledge of processes in porous media. The experiments of Andreani et al. (2009) on sintered olivine aggregates with a grain diameter of approximately 84 μm and a porosity of 17% achieved ~3% carbonation of olivine in 7.5 h, approximately 100 times slower than predicted for powders with a grain size of 84 μm, which is consistent with an "effective grain size" of 8.4 mm. Thus, for fractured Oman peridotite with an initial grain size of 0.001 to 0.01 m and a porosity of ~1%, we might expect an effective grain size of ~1 m.

3.2. Comparison of Laboratory and Natural Olivine Carbonation Rates

Kelemen & Matter (2008) fit data on the rate of olivine carbonation during the first hour of Albany Research Center experiments on 70-μm grains, and they applied this fit to reaction over periods of years at an effective grain size of ~1 m. The fit predicts that reaction at 30°C and 0.0004 bar P_{CO_2} (atmospheric P_{CO_2}) is approximately one million times slower than at 185°C and 150 bar P_{CO_2}. This prediction can be compared with natural rates. In the near-surface peridotite of Oman, we estimate CO_2 uptake of $\sim 5 \times 10^5$ tons per year (**Supplemental Table S1** and **Section S4**). The peridotite has an exposed surface area of ~5,250 km^2. If olivine carbonation due to weathering takes place mainly in a horizon ~15 m thick, as inferred from ^{14}C ages and erosion rates in Oman, it corresponds to uptake of ~1 gm CO_2 per cubic meter per year (mass fraction of $\sim 10^{-14}$ s^{-1}), which is approximately one million times slower than the predicted rate of 1 ton per cubic meter per year. Thus, laboratory and natural data agree surprisingly well (**Figure 5**).

In contrast, Wilson et al. (2009) infer carbonation rates of $\sim 10^{-10}$ s^{-1} in serpentinite mine tailings in Canada. This rapid rate, compared with olivine carbonation in laboratory studies and in Oman, probably results from the fine-grained, fibrous nature of the serpentinite mine tailings. For additional discussion, please see **Supplemental Section S10**.

4. "PHYSICAL KINETICS" OF MINERAL CARBONATION: SELF-LIMITING REACTIVE FLOW VERSUS REACTION-DRIVEN CRACKING

4.1. Volume Changes During Natural Peridotite Hydration and Carbonation

As can be seen from the simplified reactions in Section 2.2, hydration of olivine consumes water to produce serpentine and brucite, whereas complete carbonation of olivine produces magnesite

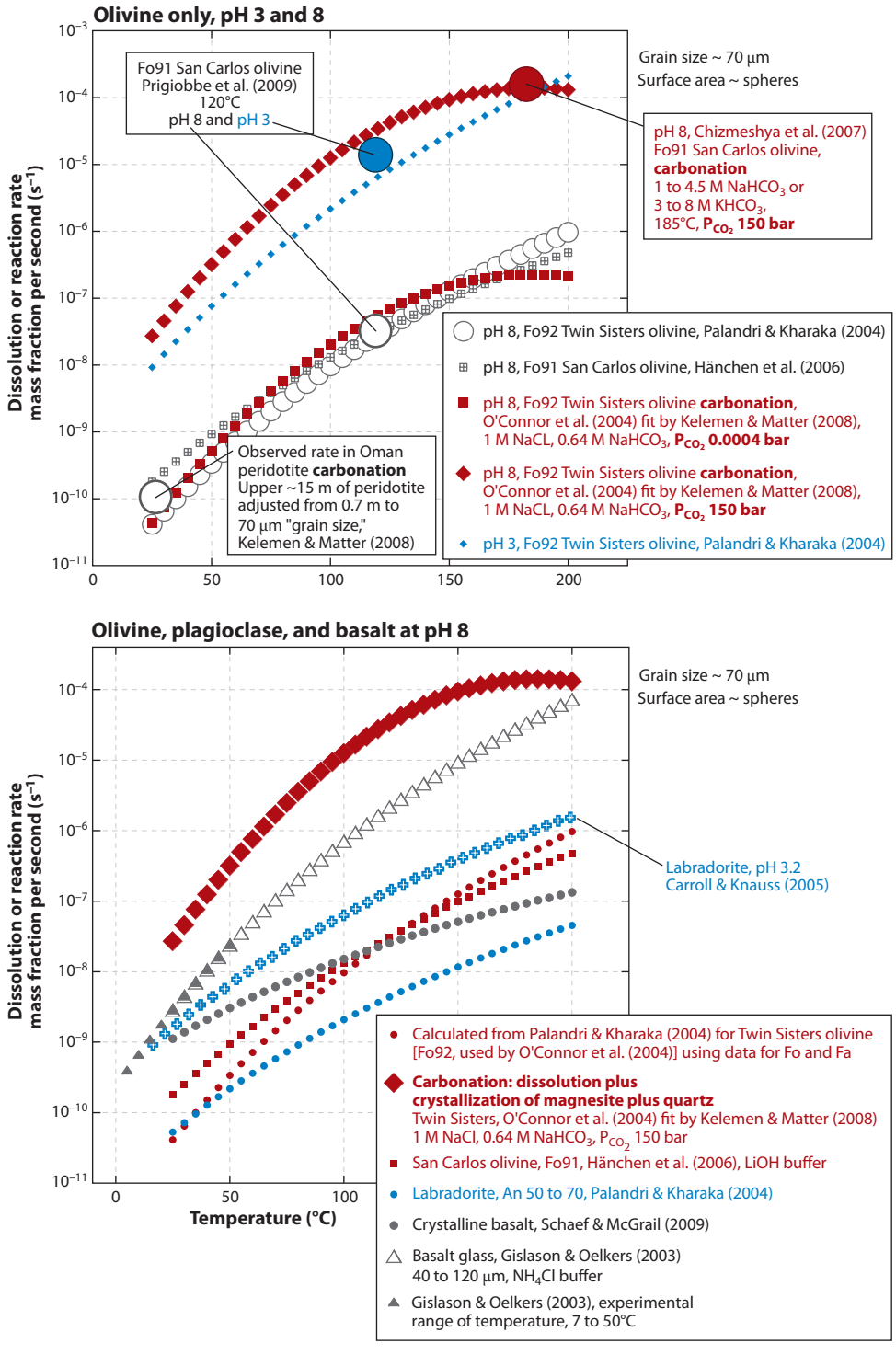

and quartz. These reactions, as written, consume fluid components to increase the solid volume by 33% (serpentinization) to 44% (carbonation) relative to the initial solid volume, in a manner similar to the hydration of lime, CaO, to form portlandite, $Ca(OH)_2$, with a 50% volume increase.

Many reactions in metamorphic rocks occur at conditions of constant volume [see the recent review by Putnis (2009)]. In principle, one could write hydration and carbonation reactions that conserve the solid volume, by positing that large amounts of solid material are dissolved and transported elsewhere in an open system. Obviously, most or all the Mg and Ca in peridotite-hosted carbonate veins and travertines has been extracted from peridotite. However, it is not apparent whether small proportions of Mg and Ca are extracted from large masses of rock or whether large proportions are extracted from small masses. Although there are exceptions (notably Snow & Dick 1995), most studies of peridotite alteration conclude that it is nearly isochemical for all major components except for the addition of H_2O and CO_2 (e.g., Andreani et al. 2007; Augustin et al. 2008; Coleman & Keith 1971; Evans 2008; Hansen et al. 2005; Kelemen et al. 2004, 2007; Robinson et al. 2005; Shervais et al. 2005). Experimentally, Andreani et al. (2009) demonstrated that peridotite carbonation in an open system produced an increase in the solid volume, despite dissolution and export of small amounts of Si, Mg, and Ca in the fluid.

Most of our samples from Oman—predominantly veins and travertine—are not appropriate for assessing the extent of mass transfer from the peridotite protolith. However, a few samples can be used. **Figure 6** compares typical analyses of partially hydrated peridotites from the mantle section of the Samail ophiolite (Hanghøj et al. 2010) with our new analyses of listwanites and partially carbonated peridotites. These samples have more variable Mg# than do typical Oman peridotites but approximately the same SiO_2 contents. Variable Mg#'s probably reflect extraction of small proportions of Mg and Ca that formed carbonate veins elsewhere. The volume decrease associated with Mg and Ca loss would have been less than 1% for most samples, whereas hydration and carbonation caused solid volume increases of more than 10%.

4.2. Self-Limiting Versus Self-Cracking Regimes: Force of Crystallization and Relaxation Mechanisms

Fluid-rock reactions that increase the solid volume are often self-limiting because they fill porosity, reduce permeability, and create reaction rims of solid products that act as diffusive boundary

Figure 5

(*Top*) Rates of olivine dissolution in aqueous fluids and of olivine carbonation in aqueous fluids with high P_{CO_2} (Chizmeshya et al. 2007, Hänchen et al. 2006, Kelemen & Matter 2008, O'Connor et al. 2004, Palandri & Kharaka 2004). Unless otherwise noted, experiments are for olivine dissolution. Although olivine dissolution can be rapid at low pH, these conditions do not favor crystallization of solid carbonate minerals. Where experimental rates were determined in units of kg m^{-2} s^{-1} or mol m^{-2} s^{-1}, they have been transformed into weight fraction per second using appropriate molecular weights, densities, and the surface areas of spheres with a diameter of 70 μm. In general, rates were calculated for reaction at pH 8. The choice of a 70-μm grain size and pH 8 was dictated by the desire to compare other data with those of O'Connor et al. (2004) and Chizmeshya et al. (2007), who did not determine surface area and/or pH dependency in their experimental studies of olivine carbonation rates. (*Bottom*) Mineral and rock dissolution rates and carbonation rates (data sources as for top panel, plus Carroll & Knauss 2005, Gislason & Oelkers 2003, Schaef & McGrail 2009). As for top panel, rates were calculated at pH 8. All data are for dissolution rates in aqueous fluid, unless the legend notes that experiments included carbonation. As for top panel, dissolution rates are rapid at low pH, but carbonate minerals are less stable in these conditions. "Fo" followed by a number refers to the molar percentage of the forsterite end-member in the mineral olivine, which is a solid solution between forsterite (Mg_2SiO_4) (Fo) and fayalite (Fe_2SiO_4) (Fa).

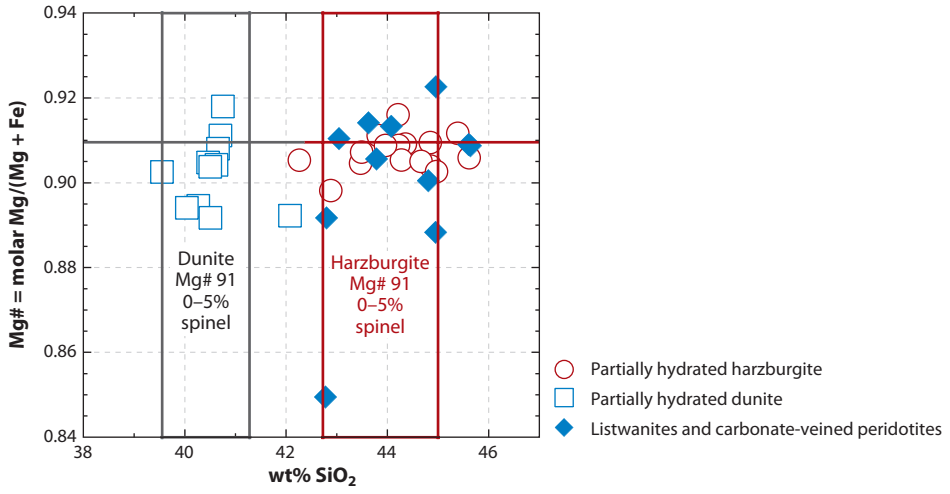

Figure 6

Bulk compositions of our listwanite and partially carbonated peridotite samples, compared with those of typical Oman peridotites from Hanghøj et al. (2010). To filter out samples containing abundant, massive carbonate veins, we eliminated those with more than 35 wt% $H_2O + CO_2$ ("loss on ignition") and with molar Ca/(Ca + Mg + Fe) greater than 0.1.

Supplemental Material

layers between unreacted mineral reactants and fluid (e.g., Aharonov et al. 1998, Milsch et al. 2009, Morrow et al. 2001, Tenthorey et al. 1998). Decreasing permeability with reaction progress is commonly observed for hydration and carbonation of basalt (Alt & Teagle 1999, Bartetzko 2005, Becker & Davis 2003, Schramm et al. 2005). On shorter timescales and distance scales, experimental dissolution and carbonation of olivine commonly show a rate decrease with time (**Supplemental Figure S4**). This arises, at least in part, from formation of a "passivating layer" of amorphous SiO_2 on olivine surfaces, after which reaction is limited by diffusion through this solid layer (e.g., Chizmeshya et al. 2007).

Alternatively, precipitation of minerals in pore space can fracture rocks, maintaining permeability and exposing fresh mineral surfaces. For example, salts crystallizing from water in limestone and other building materials can fracture these materials, even while the fluid volume is decreasing. [See the extensive literature on salt weathering, recently reviewed by Scherer 1999, 2004 and Steiger 2005a,b; also see the image at **http://web.mac.com/gwscherer1/SchererGroup/Salt_Crystallization.html.]** Frost heaves and frost cracking are related phenomena (e.g., Walder & Hallet 1985). Similarly, reaction between fluids and minerals that consume both solid and fluid components but increase the solid volume, such as hydration of solid lime (CaO) to produce portlandite [$Ca(OH)_2$], can cause polycrystalline rocks to fracture (G.W. Scherer, personal communication, 2009; also see the image at **http://web.mac.com/gwscherer1/SchererGroup/Slaking_lime.html**). This process is analogous to peridotite hydration and carbonation.

Numerous studies, beginning with Correns (Correns 1949, Correns & Steinborn 1939), demonstrated that crystal growth from a fluid in pore space, driven by surface energy and diffusion of components in a nanofilm along the contact between a growing crystal and its host, leads to local stresses in excess of the confining pressure, proportional to the extent of supersaturation of the growing mineral. In the simplest formulation, the force of crystallization or crystallization pressure is given by

$$\Delta P = RT / V_m \ln(c/c^0), \quad (3)$$

where R is the gas constant, T is the temperature in Kelvin, V_m is the molar volume of the growing crystalline phase, c is the concentration of a solute, and c^0 is the equilibrium concentration at which fluid is saturated in the growing crystalline phase. Steiger (2005a) notes that the formulation using c/c^0 is correct only for ideal solutions in which the crystal forms from a single fluid component. Given that the reaction quotient, Q, is the product of activities of reactants divided by the product of activities of products, whereas the equilibrium constant, K, is the reaction quotient for a system in equilibrium, c/c^0 should be replaced with the reaction quotient divided by the equilibrium constant. The ratio Q/K is the saturation state, Ω, so the new equation is

$$\Delta P = RT/V_m \ln(\Omega). \quad (4)$$

Steiger (2005a) calculates overpressures of hundreds of bars to kilobars for crystallization of supersaturated NaCl in pore space. For magnesite crystallization, Ω is defined by

$$\Omega = (a_{Mg++}a_{CO3-})/K_{MgCO3}. \quad (5)$$

Recent studies of (notoriously sluggish) magnesite crystallization kinetics (Hänchen et al. 2008, Saldi et al. 2009) found that $(a_{Mg++}\ a_{CO3-})/K_{MgCO3}$ can reach 100 or more at temperatures up to 120°C, yielding crystallization pressures up to 5 kbar, which is more than sufficient to fracture crustal rocks.

Because we often work with samples for which we do not know the saturation state of metamorphic fluids, the ability to estimate crystallization pressures without knowing the fluid composition would be useful. Because the standard-state free energy for a given reaction is $\Delta G^0 = -RT\ln(K)$, the free energy change for a reaction can be expressed as

$$\Delta G = -RT\ \ln(K) + RT\ \ln(Q) = RT\ \ln(\Omega), \quad (6)$$

so ΔP is now given by

$$\Delta P = \Delta G/\Delta V_s, \quad (7)$$

where ΔV_s is the solid volume change due to reaction, per mole of solid products. Equations 3–7 were developed for crystallization of a solid phase that forms entirely from solutes in fluid. For fluid-rock reactions involving dissolution of a solid reactant as well as crystallization of solid products, the volume used in the denominator of Equation 7 should probably be ΔV_s, as written, rather than the molar volume of the crystallizing phase(s).

Olivine is far from equilibrium with CO_2-rich fluids at shallow crustal conditions. If we ignore olivine dissolution kinetics for the moment, when a CO_2-rich fluid first comes into contact with olivine, there is a chemical potential driving the reaction to form magnesite + quartz, which is the free energy change of Reaction 1c. Using this free energy in Equation 7 provides an upper bound on the crystallization pressure, illustrated in **Figure 7**. In practice, slow olivine dissolution coupled with magnesite + quartz precipitation limits the saturation state, the free energy of magnesite + quartz crystallization from fluid, and the crystallization pressure to lower values. Nonetheless, these simple calculations show that there is more than enough energy, expressed as free energy/volume or pressure, to fracture rocks when olivine reacts with CO_2-rich fluids.

Reaction-driven cracking may be most likely during rapid crystallization because increasing stress in the host rock competes with slow relaxation mechanisms such as dislocation creep within growing crystals. For example, in experiments on crystallization of Na-sulfate salts in porous limestone, rapid crystallization caused fractures, whereas slow crystallization did not (Espinosa Marzal & Scherer 2008). The stress required to fracture the unconfined limestone blocks at atmospheric pressure is ~1 MPa. Salts have low viscosity (e.g., Spiers et al. 1990), and 1-MPa stresses relax in microseconds to minutes for 1–100-μm salt crystals. Thus, increasing stress due

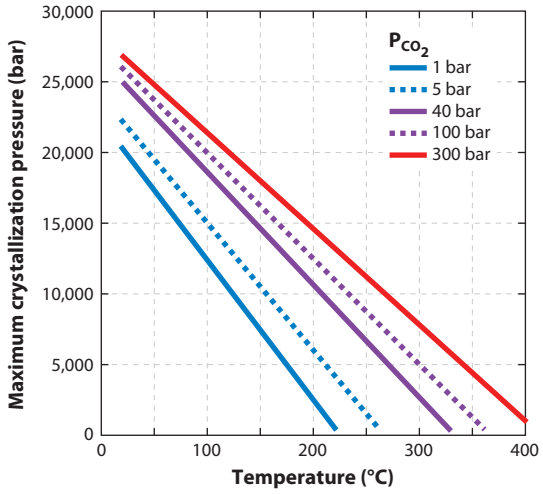

Figure 7

Maximum possible crystallization pressures, $\Delta G/\Delta V_s$, for the complete reaction of forsterite + CO_2 = magnesite + quartz in the system MgO-SiO_2-CO_2, as a function of temperature and pressure, ignoring the rates of olivine dissolution and magnesite crystallization. In practice, slow olivine dissolution, coupled with magnesite + quartz precipitation, limits the extent of fluid oversaturation in magnesite and quartz and thus limits crystallization pressures to lower values.

to salt crystallization in pore space had to take place in seconds to minutes to produce fracture rather than viscous flow of salt. Unfortunately, the steady-state viscosity of carbonate minerals at low temperature is not known (Liteanu & Spiers 2009), so we cannot quantify viscous relaxation times for carbonate growth in peridotite pore space.

In addition to being likely during rapid crystallization, reaction-driven cracking may also be favored when fluid flow takes place periodically, as may be common in arid areas subject to occasionally heavy rainfall. As noted by Scherer (2004), rapid evaporation of isolated fluid pockets in pore space drives increasing solute concentrations and potentially extreme supersaturation. This, in turn, could produce very high pressures of crystallization.

4.3. Reaction-Driven Cracking in Natural Olivine Hydration and Carbonation

The idea of reaction-driven cracking has been applied, qualitatively, to olivine hydration. MacDonald & Fyfe (1985) proposed that increasing solid volume during olivine hydration produces stresses that fracture surrounding rock. This was further investigated and quantified for serpentinization (e.g., Andreani et al. 2007; Evans 2004; Iyer et al. 2008; Jamtveit et al. 2008, 2009; O'Hanley 1992; Royne et al. 2009; Shervais et al. 2005), olivine carbonation (Rudge et al. 2010), and granite weathering (Fletcher et al. 2006). Evans (2004) and Jamtveit et al. (2008) emphasize textural evidence for reaction-driven cracking, in which partial serpentinization of olivine has shattered surrounding plagioclase crystals.

Conversely, peridotite hydration may reduce permeability and limit serpentinization (Cipolli et al. 2004, Lowell & Rona 2002). Martin & Fyfe (1970) observed experimental serpentinization rates decreasing with time, which they attributed to armoring of olivine surfaces with serpentine reaction products. Emmanuel & Berkowitz (2006) modeled this process. Similarly, the models of Xu et al. (2004) assumed that olivine carbonation gradually filled pore space and reduced permeability. O'Connor et al. (2004) observed a ~3× decrease in the rate between 26% and

93% olivine carbonation (**Supplemental Figure S4**), and Chizmeshya et al. (2007) observed a "passivating," SiO_2-rich reaction rim on olivine surfaces, formed during dissolution coupled with crystallization of magnesite + quartz.

Extensive outcrops of serpentinite indicate that olivine hydration is not always self-limiting. The ubiquitous presence of dense fracture networks that host serpentine veins in partially serpentinized peridotite, with ~10-μm spacing, lends credence to the idea that serpentinization and cracking are coeval. Without the presence of serpentine "glue" along these fracture networks, the host would be a powder rather than a rock. Furthermore, it is common to observe several generations of cross-cutting serpentine veins, which indicate repeated cycles of fracturing followed by hydration. However, fracture filling by reaction products ultimately may have limited reaction progress, where we observe partially serpentinized rocks.

Similarly, the presence of extensive outcrops of listwanite demonstrates that peridotite carbonation is not always self-limiting. Listwanites have brecciated textures in outcrop and dense, hierarchical fracture networks extending to microscopic scales, filled by synkinematic carbonate and quartz veins (**Figure 8**). Outcrop scale and microscopic relationships in partially carbonated peridotites indicate coeval carbonate crystallization and fracture. Also, geochronological data

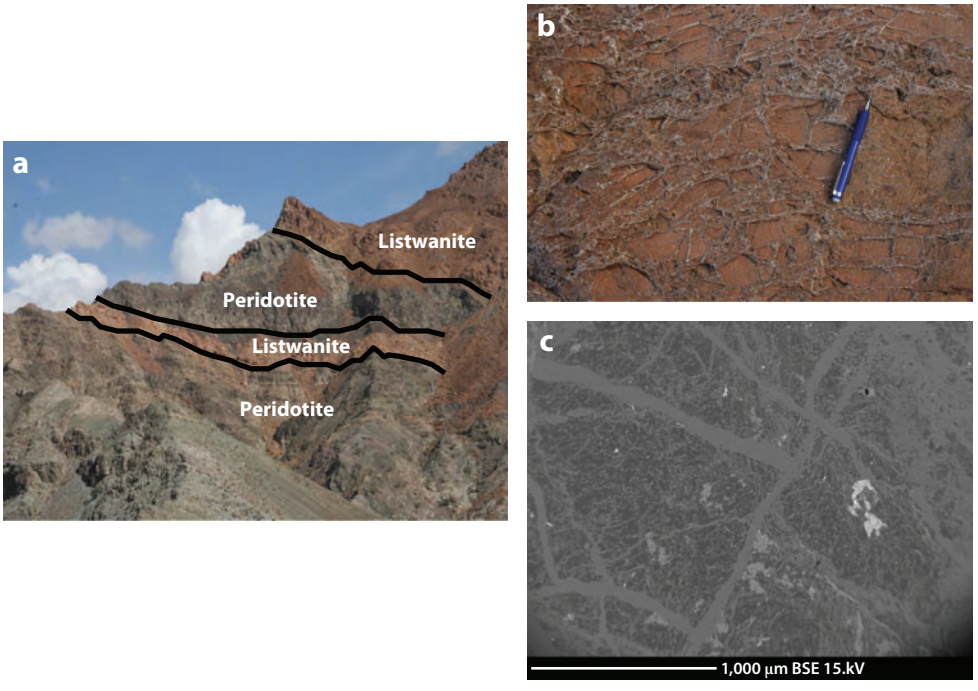

Figure 8

Outcrop and thin-section scale photographs of listwanites replacing peridotite in the ophiolite massifs of northern Oman. (*a*) Gently eastward-dipping listwanite band ~10 m in true thickness, approximately parallel to banding in partially serpentinized peridotite, and overlying, thicker band of listwanite along ridge in Oman at approximately 23.37°N, 58.19°E. This area is structurally just a few hundred meters from the basal thrust, juxtaposing peridotite with ophiolitic mélange and underlying sedimentary conglomerates in this region. [P.B. Kelemen photo, field of view (fov) 500 m.] (*b*) Typical quartz vein texture in listwanite talus block, same location. (P.B. Kelemen photo, fov 0.5 m.) (*c*) Backscattered electron (BSE) image of listwanite from same location. Dark gray indicates magnesite, light gray indicates quartz, and white indicates relict chromian spinel. (E. Streit photo, fov 0.0025 m.)

(^{14}C, U-series) show that permeability is maintained over tens of thousands of years in water-peridotite systems undergoing carbonation and serpentinization, both in Oman (Kelemen & Matter 2008) and in the Lost City hydrothermal vent field along the Mid-Atlantic Ridge (Früh-Green et al. 2003, Ludwig et al. 2006).

Supplemental Material

Carbonate veins in Oman peridotites commonly occur in three mutually perpendicular vein sets (**Figure 9** and **Supplemental Section S11**), suggesting that they formed in a nearly isotropic stress regime and not because of tectonic compression or extension. Nearly horizontal fractures roughly parallel to the paleooutcrop surface predate a second set of nearly vertical fractures perpendicular to the outcrop surface (**Figure 9**). This is consistent with models in which volume expansion in a diffusive reaction zone drives fracture parallel to the weathering surface and is followed by buckling of the detached, weathered layer and subsequent cracking perpendicular to the weathering surface (Fletcher et al. 2006, Rudge et al. 2010).

Rudge et al. (2010) predict that propagation of a cracking front associated with peridotite hydration and carbonation is a function of the reaction rate and the reactant transport velocity in pore space. On the basis of this work, we estimate that reaction at elevated temperature and P_{CO_2}, with approximately 1% initial fracture porosity and fluid flow velocities of ~0.01 m s^{-1}, can drive propagation of a cracking front at velocities of meters per day (**Figure 10**). However, the formulation of Rudge et al. (2010) is calibrated only to the average erosion rates estimated from thermochronology of samples (from lithologies other than peridotite) in the Oman mountains (Poupeau et al. 1998).

Finally, as pointed out by Cipolli et al. (2004) and Hansen et al. (2005), partial carbonation of serpentine rather than olivine, via Reactions 1e and 1f, does not involve a large change in the solid volume, yet it consumes substantial quantities of CO_2. Thus, this process might not have a large effect on porosity and permeability. However, it involves a small enthalpy change, so potential positive feedbacks due to exothermic heat production are not important. Also, serpentine carbonation—without expensive heat treatment to ~600°C prior to reaction—is more than 10 times slower than olivine carbonation under similar conditions of temperature, fluid composition, and P_{CO_2} (e.g., Gerdemann et al. 2007, O'Connor et al. 2004).

5. ENGINEERED, IN SITU PERIDOTITE CARBONATION FOR CO_2 CAPTURE AND STORAGE

Kinetic data summarized in Section 3 show conversions from olivine to magnesite + quartz (Reaction 1c) of ~50% per hour. However, even at these rapid conversion rates, the cost of ex situ olivine or serpentine carbonation—quarrying peridotite, transporting it to a concentrated source of CO_2 such as a fossil fuel–burning power plant, grinding it to ~70 μm in size, and reacting it with fluids at high P_{CO_2} and high temperature—may not be low enough for industrial implementation, although development work continues (Mazzotti et al. 2005).

As an alternative, Schuiling & Krijgsman (2006) proposed avoiding the cost of high-pressure, high-temperature reaction vessels via spreading fine-grained olivine powder over agricultural and forest land or along beaches. The efficacy of this method has been questioned on energetic and environmental grounds (Hangx & Spiers 2009).

Another alternative is in situ carbonation of olivine, in which CO_2-rich fluid is transported to areas where large volumes of peridotite are present near the surface (Cipolli et al. 2004, Guthrie et al. 2001, Hansen et al. 2005, Kelemen & Matter 2008, Kelemen et al. 2008, Marini 2007, Matter & Kelemen 2009, Schuiling 2006, Xu et al. 2004). Kelemen & Matter (2008) suggested two end-member methods for rapid, cost-effective peridotite carbonation for CO_2 storage:

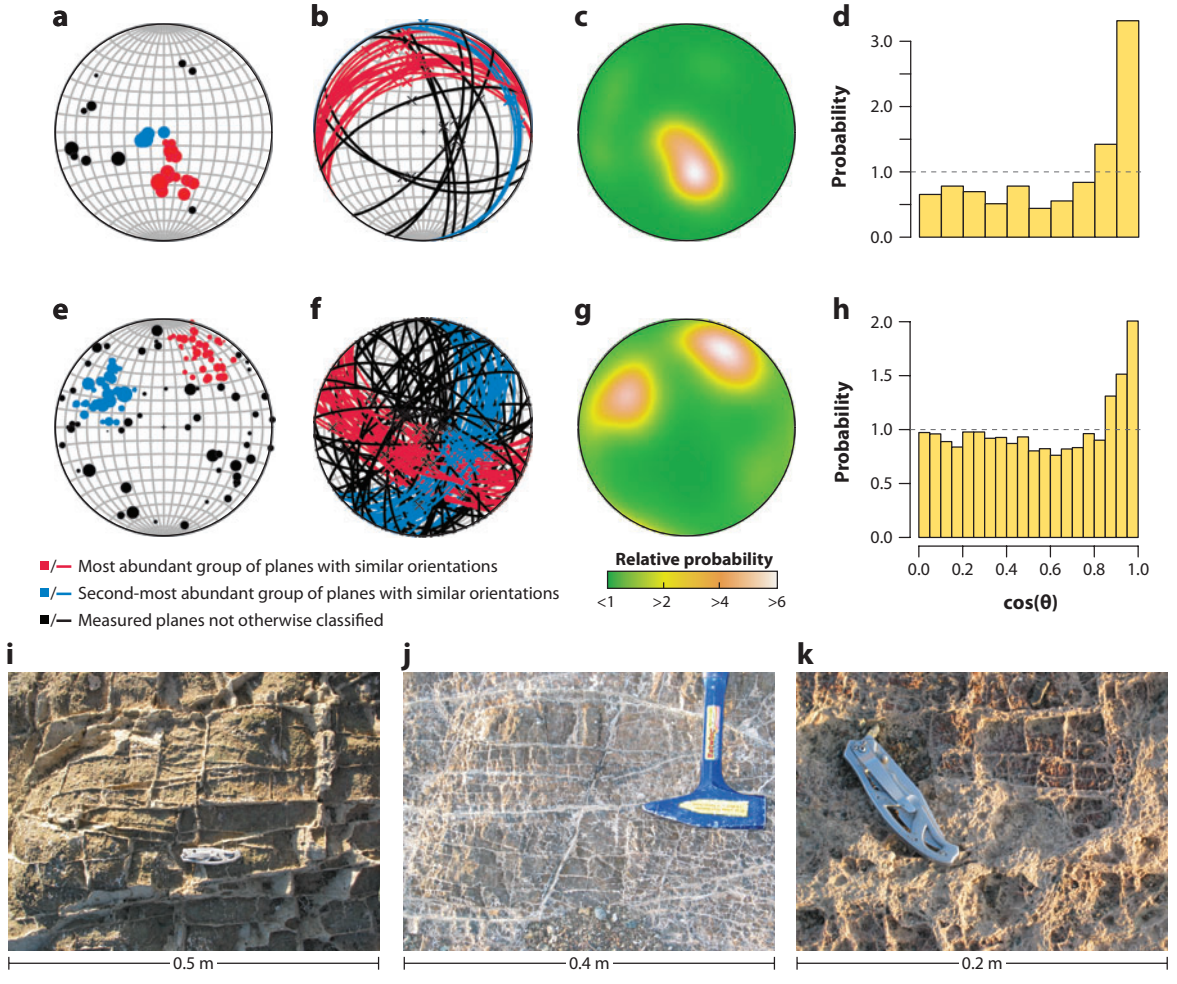

Figure 9

(*a–b*) Stereoplots and histograms: orientations of tabular carbonate veins in peridotite near a large travertine deposit in northern Oman, at approximately 21.86°N, 57.51°E. Panels *a–d* are for measurements of vein orientations measured on nearly vertical outcrop surfaces; panels *e–h* are for vein orientations measured on a nearly horizontal outcrop surface nearby. Red symbols and lines are for all planes that have poles within 25° of the density maximum. Blue symbols and lines are for all planes that have poles within the second density maximum, after the data with red symbols have been removed from the data set. (*a*,*e*) Poles to planes, projected on a lower-hemisphere stereonet. (*b*,*f*) Planes projected on a lower-hemisphere stereonet. (*c*,*g*) Contoured density of poles using a von Mises kernel with $\kappa = 10$, projected on a lower-hemisphere stereonet. Relative probabilities are <1 for the green region, more than 2 for the yellow region, more than 4 for the brown region, and more than 6 for the white region. (*d*,*h*) Histograms of intersection angles; 90° intersections are the best-represented group in both data sets. There are few intersections of steeply dipping veins with the steep outcrop surfaces of panels *a–d* and few intersections of nearly horizontal veins with the subhorizontal surfaces of panels *e–h*. If the two data sets were equal in size, one could combine them to produce a statistical representation of the three mutually orthogonal vein sets that constitute a majority of the carbonate veins in this area. (*i–k*) Outcrop-scale, hierarchical networks of carbonate veins in peridotite near a large travertine deposit in northern Oman, at approximately 21.86°N, 57.51°E (as for data in stereoplots and histograms). Photographs of nearly vertical outcrop surfaces on small canyon walls, showing progressively smaller and more closely spaced carbonate veins from left to right. Thin sections from panels *i* and *j* show sharp-sided carbonate veins in a partially serpentinized peridotite host containing little or no carbonate and 20–40% fresh olivine. In bottom half of panel *k*, peridotite is 100% replaced by carbonate. Note orthogonal vein intersections, and the fact that subhorizontal veins are larger than subvertical veins. The subhorizontal fractures that host veins formed mainly before the subvertical fractures that host veins because the steep fractures commonly terminate where they intersect with the nearly horizontal fractures.

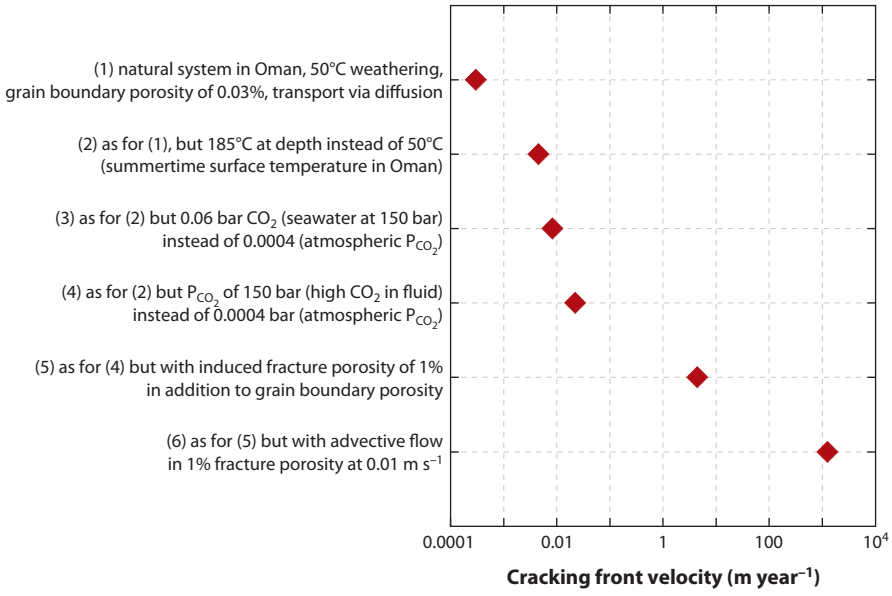

Figure 10

Rate of propagation of a reaction-driven fracture network due to increasing solid volume during peridotite carbonation, calculated using the formulation of Rudge et al. (2010).

- Method 1: A rock volume at depth is raised to the optimal temperature for olivine carbonation (~185°C), hydraulically fractured, and injected with fluids (with added $NaHCO_3$ if necessary) that are equilibrated with CO_2 at ~100 bar.
- Method 2: A high-temperature rock volume at depth is hydraulically fractured to induce thermal convection of seawater through peridotite.

5.1. Method 1: Injection of High-P_{CO_2} Aqueous Fluid into Preheated Peridotite for CO_2 Storage

Assuming that the surface-area-to-volume relationship for 70-μm particles in kinetic experiments can be approximated as it is for spheres or cubes, scaling to a grain size or crack spacing of ~0.7 m (surface area per unit volume 10^{-4} times that for 70-μm grains) yields olivine carbonation rates of ~50% per year in reaction with bicarbonate-rich aqueous solutions at 185°C and 150 bar P_{CO_2} (Kelemen & Matter 2008). Given an olivine density of ~3.3 tons per cubic meter and consumption of 0.62 tons of CO_2 per ton of olivine reactant, 50% carbonation of olivine corresponds to solidification of ~1 ton of CO_2 per cubic meter per year. At this rate, a cubic meter of olivine (~3.3 tons) would be converted to magnesite + quartz in two years, consuming two tons of CO_2. As shown by Kelemen & Matter (2008), such reaction rates are fast enough that heat evolved via the exothermic carbonation reaction offsets cooling due to injection of cold fluid and to diffusion into colder, surrounding rocks. Thus, energy may be required to raise a target rock volume to 185°C, but afterward this optimal temperature can be maintained by balancing the fluid flow rate with the exothermic heat output from carbonation and hydration reactions.

Compared with ex situ mineral carbonation, Method 1 avoids the cost of quarrying and transporting peridotite, grinding it, and reacting it with fluid at elevated temperature and P_{CO_2} in a pressure vessel. For a site used to store millions to billions of tons, the cost of initial

hydrofracture per ton of CO_2 could be small, and reaction-driven cracking might maintain permeability and reactive surface area. However, Method 1 adds the cost of preheating rock to ~185°C. An estimation of this cost is provided in **Supplemental Section S12**. If heating is done using oil, at $80 per barrel (i.e., ~$0.50 per kilogram of fuel), heating would cost $8 to $41 per ton of CO_2 stored. This would be an added cost compared with that of industrial CO_2 capture coupled with injection into subsurface pore space. If one reacting rock volume can heat an adjacent volume by diffusion, then the heating costs for that adjacent volume could be substantially smaller.

5.2. Method 2: Enhanced Convection of Seawater Through Peridotite for CO_2 Capture and Storage

Continued increases in atmospheric CO_2 [at and above predicted rates (e.g., online updates by the Global Carbon Project to Raupach et al. 2007)], together with slow progress on limiting or mitigating CO_2 emissions in the future, render it likely that atmospheric CO_2 will reach 500 ppmv or more. This may be too high to sustain an acceptable standard of living. Thus, "negative CO_2 emissions" may become necessary. Such negative emissions cannot be attained by carbon capture at fossil fuel power plants, which at best can only approach zero emissions.

Induced convection of seawater through peridotite, Method 2, offers an in situ alternative that achieves negative emissions and avoids the cost of industrial CO_2 capture and transport, as well as the cost of manufacturing or processing reagents. Use of seawater rather than purified CO_2 would also mitigate health risks associated with possible CO_2 leaks. Reaction with peridotite would remove almost all dissolved carbon from the water, as in natural hydrothermal systems (**Figure 11**). CO_2-depleted water would return to the sea surface via production wells. Once at the surface or near surface, the CO_2-depleted, slightly alkaline water would mix with ambient seawater and depress the seawater's near-surface partial pressure of CO_2. This enhanced air-sea

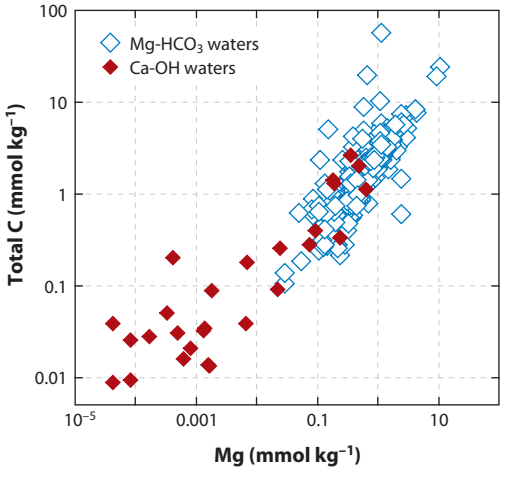

Figure 11

Mg and C concentrations in Mg-HCO_3 fluids (surface water, groundwater) and Ca-OH fluids (alkaline spring waters) from peridotite-hosted aquifers. Reaction progress is from upper right to lower left, as reaction between Mg-HCO_3 fluids and peridotite forms Mg-carbonate minerals and serpentine plus Mg- and C-depleted Ca-OH waters. Data from Barnes & O'Neil (1969), Barnes et al. (1978), Bruni et al. (2002), Launay & Fontes (1985), Matter et al. (2006), Neal & Stanger (1985), O'Neil & Barnes (1971), Weyhenmeyer (2000), and L. Marini (personal communication, 2009).

gradient of CO_2 partial pressure would draw down atmospheric CO_2, with a time constant of approximately one year (W. Broecker, personal communication, 2009).

The method is simple: Drill holes, create a network of hydraulic fractures, and induce thermal convection of seawater from the resulting holes and fracture network through peridotite and back to the sea surface, or at least to the shallow seafloor. Pumping seawater would be costly, per kilogram of CO_2 consumed, because seawater has a total carbon concentration—expressed as CO_2—of ~100 ppm by weight, so it is necessary to rely on thermal convection as much as possible. Regions with high heat flow would be ideal. Offshore drilling is approximately 10 times more costly than on land, but there are advantages to offshore CO_2 storage of any kind (e.g., Schrag 2007). Thus, it would be best to drill inclined holes from a shore-based platform into peridotite beneath adjacent, shallow seafloor. Electric power generation as a by-product seems possible because the convection cycle we invoke is essentially a geothermal power system. In fact, because it is undesirable to return geothermally heated water to the environment, use of excess heat to generate electricity might be necessary even if it is not profitable for the power generation alone.

Unlike injection of CO_2-rich fluid, CO_2 uptake via injection of seawater into peridotite would be limited by CO_2 supply to a given volume of peridotite rather than by the reaction rate, regardless of temperature, as shown in **Supplemental Section S14**. In turn, the CO_2 supply rate is limited by the permeability of fractured peridotite (**Supplemental Section S15**) or by the maximum practical flow rate in drill pipe. In the latter case, an average flow velocity of $\leq$20 m s^{-1} in a 13-inch (17-cm) pipe yields a seawater flux of $\leq$2 m^3 s^{-1}. Thus, such a system might consume up to 6,000 tons of CO_2 per year per drill hole. Maximum fluid velocities attained so far in enhanced geothermal systems that are sited in crystalline rocks are only ~0.3 m s^{-1}, with a tenfold improvement projected over the next decade (e.g., Genter et al. 2010). A flow velocity of 3.5 m s^{-1} would result in consumption of 1,000 tons of CO_2 per year per drill hole.

Supplemental Material

Although cooling due to injection of fluid would no longer be balanced by exothermic heat production, because of slower olivine carbonation rates, low fluid fluxes would yield very slow cooling of the reacting volume, and in any case the reaction rate would not limit CO_2 uptake, even at low temperature. As a result of slow reaction rates, filling of pore space and armoring of reactive surfaces might be a relatively small problem for Method 2 compared with Method 1.

Because it would involve only drilling and hydrofracture (no preheating of rock volume, no CO_2 transport, no industrial CO_2 capture, and no pumping of fluid), and because it would be combined with geothermal power generation, this process might be less costly than in situ carbonation using purified CO_2—and possibly even less costly than injection of supercritical CO_2 into underground pore space. If the net cost to engineer and maintain a system consuming ~1,000 tons of CO_2 per year for 10 years, minus the revenues from geothermal power generation, were $100,000 to $1 million, this would correspond to a cost of ~$10 to $100 per ton of CO_2. This is a total cost, for comparison with the combined cost of industrial CO_2 capture, transport, and storage. Because individual drill holes can transport only a fixed amount of water, scaling up this process simply requires more holes. Consuming one billion tons of CO_2 per year would require one million drill holes of this type, equivalent to the current number of producing oil and gas wells in the United States (**http://img36.imageshack.us/img36/9106/oilgasmaplg.jpg**).

6. FROM OBSERVATIONS TO SOLUTIONS

Enhanced, in situ carbonation of olivine in peridotite shows theoretical promise as a method of CO_2 storage and for CO_2 capture from seawater. It may be possible to capitalize on the exothermic nature of olivine carbonation to reach a positive feedback regime that maintains high temperatures

and reaction rates in selected rock volumes at depth, and to harness the large increase in solid volume to access a regime in which stress increase due to expansion forms fractures, maintaining permeability and reactive surface area for relatively long periods of time. The presence of naturally formed, fully carbonated peridotite deposits (listwanites) attests to the fact that peridotite carbonation can continue to completion. Furthermore, documented cases of ongoing peridotite carbonation demonstrate that such processes can continue for tens of thousands of years.

That said, the physical and chemical regimes required to sustain rapid reaction rates and sufficient fluid flow are not well constrained. Rapid fluid flow can cool rock volumes and thus "quench" reaction rates. Precipitation of carbonate minerals in pore space can reduce permeability and/or armor reactive surfaces. The presence of partially carbonated peridotites, typically composed of carbonate veins that cut blocks of partially hydrated, partially fresh peridotite, may provide examples of self-limiting carbonation processes.

Thus, continued research—via field studies of natural systems, laboratory experiments, and pilot experiments in drill holes—should focus on delineating the parameter ranges that define both positive and negative feedback regimes for peridotite carbonation. Reaction-driven cracking is of particular importance. At this stage, numerous approximations and extrapolations are needed to make more accurate, quantitative predictions of fracture formation or propagation rates. If a rock volume undergoing olivine carbonation enters the self-cracking regime, then the potential costs of repeated hydraulic fracture for in situ carbonation, or of grinding solid reactants for ex situ carbonation, can be avoided.

Finally, injection of seawater rather than CO_2-rich fluids avoids the cost of industrial CO_2 capture and provides a method for negative CO_2 emissions. The process may be so much less expensive than injection of CO_2-rich fluids that other drawbacks are minor.

DISCLOSURE STATEMENT

P.B. Kelemen and J. Matter have a provisional patent filing on the methods for CO_2 capture and storage via mineral carbonation that are described in their 2008 paper in the *Proceedings of the National Academy of Sciences*. Other than that, the authors are not aware of any affiliations, memberships, funding, or financial holdings that might be perceived as affecting the objectivity of this review.

LITERATURE CITED[1]

Abart R, Pozzorini D. 2000. Implications of kinetically controlled mineral-fluid exchange on the geometry of stable-isotope fronts. *Eur. J. Mineral.* 12:1069–82

Agrinier P, Cornen G, Beslier M-O. 1996. Mineralogical and oxygen isotopic features of serpentinites recovered from the ocean/continent transition in the Iberia abyssal plain. In *Proceedings of the Ocean Drilling Program, Scientific Results*, Vol. 149, ed. RB Whitmarsh, DS Sawyer, A Klaus, DG Masson, pp. 541–52. College Station, TX: Ocean Drill. Program

Agrinier P, Mével C, Girardeau J. 1988. Hydrothermal alteration of the peridotites cored at the ocean/continent boundary of the Iberian margin: petrologic and stable isotope evidence. In *Proceedings of the Ocean Drilling Program, Scientific Results*, Vol. 103, ed. G Boillot, EL Winterer, pp. 225–34. College Station, TX: Ocean Drill. Program

Aharonov E, Tenthorey E, Scholz CH. 1998. Precipitation sealing and diagenesis: 2. Theoretical analysis. *J. Geophys. Res.* 103(B10):23969–81

[1]Also see additional references in the electronic supplement. View the supplement by following the **Supplemental Materials link** on the Annual Reviews home page at **http://www.annualreviews.org**.

Allen DE, Seyfried WE Jr. 2004. Serpentinization and heat generation: constraints from Lost City and Rainbow hydrothermal systems. *Geochim. Cosmochim. Acta* 68:1347–54

Alt JC, Teagle DAH. 1999. The uptake of carbon during alteration of oceanic crust. *Geochim. Cosmochim. Acta* 63:1527–35

Andreani M, Luquot L, Gouze P, Godard M, Hoisé E, Gibert B. 2009. Experimental study of carbon sequestration reactions controlled by the percolation of CO_2-rich brine through peridotites. *Environ. Sci. Technol.* 43:1226–31

Andreani M, Mével C, Boullier A-M, Escartin J. 2007. Dynamic control on serpentine crystallization process in veins: constraints on hydration processes in oceanic peridotites. *Geochem. Geophys. Geosyst.* 8:Q02012

Augustin N, Lackschewitz KS, Kuhn T, Devey CW. 2008. Mineralogical and chemical mass changes in mafic and ultramafic rocks from the Logatchev hydrothermal field (MAR 15°N). *Mar. Geol.* 256:18–29

Barbieri M, Masi U, Tolomeo L. 1979. Stable isotope evidence for a marine origin of ophicalcites from the north-central Apennines (Italy). *Mar. Geol.* 30:193–204

Barnes I, LaMarche VC, Himmelberg G. 1967. Geochemical evidence of present-day serpentinization. *Science* 156:830–32

Barnes I, O'Neil JR. 1969. Relationship between fluids in some fresh alpine-type ultramafics and possible modern serpentinization, western United States. *Geol. Soc. Am. Bull.* 80:1947–60

Barnes I, O'Neil JR, Rapp JB, White DE. 1973. Silica-carbonate alteration of serpentine: wall rock alteration in mercury deposits of the California Coast Ranges. *Econ. Geol.* 68:388–98

Barnes I, O'Neil JR, Trescases JJ. 1978. Present-day serpentinization in New Caledonia, Oman and Yugoslavia. *Geochim. Cosmochim. Acta* 42:144–45

Bartetzko A. 2005. Effect of hydrothermal ridge flank alteration on the in situ physical properties of oceanic crust. *J. Geophys. Res.* 110:B06203

Beard JS, Frost BR, Fryer P, McCaig A, Searle R, et al. 2009. Onset and progression of serpentinization and magnetite formation in olivine-rich troctolite from IODP Hole U1309D. *J. Petrol.* 50:387–403

Becker K, Davis E. 2003. New evidence for age variation and scale effects of permeabilities of young oceanic crust from borehole thermal and pressure measurements. *Earth Planet. Sci. Lett.* 210:499–508

Berndt ME, Allen DE, Seyfried WE Jr. 1996. Reduction of CO_2 during serpentinization of olivine at 300°C and 500 bar. *Geology* 24:351–54

Blank JG, Green SJ, Blake D, Valley JW, Kita NT, et al. 2009. An alkaline spring system within the Del Puerto ophiolite (California, USA): a Mars analog site. *Planet. Space Sci.* 57:533–40

Bonatti E, Lawrence JR, Hamlyn PR, Breger D. 1980. Aragonite from deep sea ultramafic rocks. *Geochim. Cosmochim. Acta* 44:1207–14

Bosch D, Jamais M, Boudier F, Nicolas A, Dautria JM, Agrinier P. 2004. Deep and high-temperature hydrothermal circulation in the Oman ophiolite—petrological and isotopic evidence. *J. Petrol.* 45:1181–208

Boudier F, Baronnet A, Mainprice D. 2010. Serpentine mineral replacements of natural olivine and their seismic implications: oceanic lizardite versus subduction-related antigorite. *J. Petrol.* 51:495–512

Bruni J, Canepa M, Chiodini G, Cioni R, Cipolli F, et al. 2002. Irreversible water-rock mass transfer accompanying the generation of the neutral, Mg-HCO_3 and high-pH, Ca-OH spring waters of the Genova province, Italy. *Appl. Geochem.* 17:455–74

Cannat M, Mével C, Maïa M, Deplus C, Gente P, et al. 1995. Thin crust, ultramafic exposure and rugged faulting patterns at the Mid-Atlantic Ridge (22°–24°N). *Geology* 23:49–52

Carlson RL. 2001. The abundance of ultramafic rocks in the Atlantic ocean crust. *Geophys. J. Int.* 144:37–48

Carroll SA, Knauss KG. 2005. Dependence of labradorite dissolution kinetics on $CO_{2(aq)}$, $Al_{(aq)}$, and temperature. *Chem. Geol.* 217:213–25

Casey J. 1997. Comparison of major- and trace-element geochemistry of abyssal peridotites and mafic plutonic rocks with basalts from the MARK region of the Mid-Atlantic Ridge. In *Proceedings of the Ocean Drilling Program, Scientific Results*, Vol. 153, ed. JA Karson, M Cannat, DJ Miller, D Elthon, pp. 181–241. College Station, TX, Ocean Drill. Program

Chacko T, Deines P. 2008. Theoretical calculation of oxygen isotope fractionation factors in carbonate systems. *Geochim. Cosmochim. Acta* 72:3642–60

Chizmeshya AVG, McKelvy MJ, Squires K, Carpenter RW, Béarat H. 2007. A novel approach to mineral carbonation: enhancing carbonation while avoiding mineral pretreatment process cost. *U.S. Dep. Energy Final Rep. 924162*, Ariz. State Univ., Tempe, Ariz.

Cipolli F, Gambardella B, Marini L, Ottonello G, Zuccolini MV. 2004. Geochemistry of high-pH waters from serpentinites of the Gruppo di Voltri (Genova, Italy) and reaction path modeling of CO_2 sequestration in serpentinite aquifers. *Appl. Geochem.* 19:787–802

Clark ID, Fontes JC. 1990. Paleoclimatic reconstruction in northern Oman based on carbonates from hyperalkaline groundwaters. *Quat. Res.* 33:320–36

Clark ID, Fontes JC, Fritz P. 1992. Stable isotope disequilibria in travertine from high pH waters: laboratory investigations and field observations from Oman. *Geochim. Cosmochim. Acta* 56:2041–50

Coleman RG, Keith TE. 1971. A chemical study of serpentinization, Burro Mountain, California. *J. Petrol.* 12:311–28

Correns CW. 1949. Growth and dissolution of crystals under linear pressure. *Discuss. Faraday Soc.* 5:267–71

Correns CW, Steinborn W. 1939. Experimente zur Messung und Erklärung der sogenannten Kristallisationskraft. *Zeit. Krist. A* 101:117–33

Dewandel B, Boudier F, Kern H, Warsi W, Mainprice D. 2003. Seismic wave velocity and anisotropy of serpentinized peridotite in the Oman ophiolite. *Tectonophysics* 370:77–94

Dewandel B, Lachassagne P, Boudier F, Al-Hattali S, Ladouche B, et al. 2005. A conceptual hydrogeological model of ophiolite hard-rock aquifers in Oman based on a multiscale and a multidisciplinary approach. *Hydrogeol. J.* 13:708–26

Eickmann B, Bach W, Rosner M, Peckmann J. 2009. Geochemical constraints on the modes of carbonate precipitation in peridotites from the Logatchev Hydrothermal Vent Field and Gakkel Ridge. *Chem. Geol.* 268:97–106

Eiler J. 2007. "Clumped-isotope" geochemistry: the study of naturally occurring, multiply substituted isotopologues. *Earth Planet. Sci. Lett.* 262:309–27

Emmanuel S, Berkowitz B. 2006. Suppression and stimulation of seafloor hydrothermal convection by exothermic mineral hydration. *Earth Planet. Sci. Lett.* 243:657–68

Espinosa Marzal RM, Scherer GW. 2008. Crystallization of sodium sulfate salts in limestone. *Environ. Geol.* 56:605–21

Evans BW. 1977. Metamorphism of alpine peridotite and serpentinite. *Annu. Rev. Earth Planet. Sci.* 5:397–447

Evans BW. 2004. The serpentinite multisystem revisited: Chrysotile is metastable. *Int. Geol. Rev.* 46:479–506

Evans BW. 2008. Control of the products of serpentinization by the $Fe^{2+}Mg_{-1}$ exchange potential of olivine and orthopyroxene. *J. Petrol.* 49:1873–87

Evans CA, Baltuck M. 1988. Low-temperature alteration of peridotite, Hole 637A. In *Proceedings of the Ocean Drilling Program, Scientific Results*, Vol. 103, ed. G Boillot, EL Winterer, pp. 235–39. College Station, TX: Ocean Drill. Program

Fallick AE, Ilich M, Russell MJ. 1991. A stable isotope study of the magnesite deposits associated with the alpine-type ultramafic rocks of Yugoslavia. *Econ. Geol.* 86:847–61

Fletcher RC, Buss HL, Brantley SL. 2006. A spheroidal weathering model coupling porewater chemistry to soil thickness during steady-state denudation. *Earth Planet. Sci. Lett.* 244:444–57

Friedman I, O'Neil JR. 1977. Compilation of stable isotope fractionation factors of geochemical interest. In *USGS Prof. Pap. 440-KK, Data of Geochemistry*, ed. M Fleischer, pp. KK1–12. Reston, VA: U.S. Geol. Surv., 6th ed.

Frost BR. 1985. On the stability of sulfides, oxides, and native metals in serpentinite. *J. Petrol.* 26:31–63

Frost BR, Beard JS. 2007. On silica activity and serpentinization. *J. Petrol.* 48:1351–68

Früh-Green GL, Kelley DS, Bernasconi SM, Karson JA, Ludwig KA, et al. 2003. 30,000 years of hydrothermal activity at the Lost City vent field. *Science* 301:495–98

Früh-Green GL, Weissert H, Bernoulli D. 1990. A multiple fluid history recorded in Alpine ophiolites. *J. Geol. Soc. Lond.* 147:959–70

Früh-Green GL, Connollly JAD, Plas A, Kelley DS, Grobety B. 2004. Serpentinization of oceanic peridotites: implications for geochemical cycles and biological activity. In *The Subseafloor Biosphere at Mid-Ocean Ridges*, ed. WSD Wilcock, EF DeLong, DS Kelley, JA Baross, SC Cary, *Geophys. Monogr.* 144:119–136. Washington, DC: AGU

Fyfe WS. 1974. Heats of chemical reactions and submarine heat production. *Geophys. J. R. Astron. Soc.* 37:213–15

Genter A, Goerke X, Graff, JJ, Cuenot N, Krall G, et al. 2010. Current status of the EGS Soultz geothermal project (France). *Proc. World Geotherm. Cong., Apr. 25–29*, Bali, Indones., pp. 1–6. Reykjavik: Int. Geotherm. Assoc.

Gerdemann SJ, O'Connor WK, Dahlin DC, Penner LR, Rush H. 2007. Ex situ aqueous mineral carbonation. *Environ. Sci. Technol.* 41:2587–93

Ghosh P, Adkins J, Affek H, Balta B, Guo W, et al. 2006. ^{13}C–^{18}O bonds in carbonate minerals: a new kind of paleothermometer. *Geochim. Cosmochim. Acta* 70:1439–56

Gislason SR, Oelkers EH. 2003. Mechanism, rates and consequences of basaltic glass dissolution: II. An experimental study of the dissolution rates of basaltic glass as a function of pH and temperature. *Geochim. Cosmochim. Acta* 67:3817–32

Greenwood HJ. 1967. Mineral equilibria in the system MgO-SiO_2-H_2O-CO_2. In *Researches in Geochemistry II*, ed. PH Abelson, pp. 542–47. New York: John Wiley & Sons

Gregory RT, Taylor HP. 1981. An oxygen isotope profile in a section of Cretaceous oceanic crust, Samail ophiolite, Oman: evidence for $\delta^{18}O$ buffering of the oceans by deep (>5 km) seawater-hydrothermal circulation at mid-ocean ridges. *J. Geophys. Res.* 86:2737–55

Guthrie GD, Carey JW, Bergfeld D, Byer D, Chipera S, et al. 2001. Geochemical aspects of the carbonation of magnesium silicates in an aqueous medium. *Proc. First Natl. Conf. Carbon Sequestration, Wash., DC*, pp. 1–14. Washington, DC: U.S. Dep. Energy Natl. Energy Technol. Lab.

Hacker BR. 1994. Rapid emplacement of young oceanic lithosphere: argon geochronology of the Oman ophiolite. *Science* 265:1563–65

Haggerty JA. 1991. Evidence from fluid seeps atop serpentine seamounts in the Mariana Forearc: clues for emplacement of the seamounts and their relationship to forearc tectonics. *Mar. Geol.* 102:293–309

Hänchen M, Prigiobbe V, Baciocchi R, Mazzotti M. 2008. Precipitation in the Mg-carbonate system: effects of temperature and CO_2 pressure. *Chem. Eng. Sci.* 63:1012–28

Hänchen M, Prigiobbe V, Storti G, Seward TM, Mazzotti M. 2006. Dissolution kinetics of fosteritic olivine at 90–150°C including effects of the presence of CO_2. *Geochim. Cosmochim. Acta* 70:4403–16

Hanghøj K, Kelemen PB, Hassler D, Godard M. 2010. Composition and genesis of depleted mantle peridotites from the Wadi Tayin massif, Oman ophiolite: major and trace element geochemistry, and Os isotope and PGE systematics. *J. Petrol.* 51:206–27

Hangx SJT, Spiers CJ. 2009. Coastal spreading of olivine to control atmospheric CO_2 concentrations: a critical analysis of viability. *Int. J. Greenh. Gas Control* 3:757–67

Hansen LD, Dipple GM, Gordon TM, Kellett DA. 2005. Carbonated serpentinite (listwanite) at Atlin, British Columbia: a geological analogue to carbon dioxide sequestration. *Can. Mineral.* 43:225–39

Holland TJB, Powell R. 1998. An internally consistent thermodynamic data set for phases of petrological interest. *J. Metamorph. Geol.* 16:309–43

Horita J, Berndt ME. 1999. Abiotic methane formation and isotopic fractionation under hydrothermal conditions. *Science* 285:1055–57

Iyer K, Jamtveit B, Mathiesen J, Malthe-Sorenssen A, Feder J. 2008. Reaction-assisted hierarchical fracturing during serpentinization. *Earth Planet. Sci. Lett.* 267:503–16

Jamtveit B, Malthe-Sorenssen A, Kostenko O. 2008. Reaction enhanced permeability during retrogressive metamorphism. *Earth Planet. Sci. Lett.* 267:620–27

Jamtveit B, Putnis C, Malthe-Sorenssen A. 2009. Reaction induced fracturing during replacement processes. *Contrib. Mineral. Petrol.* 157:127–33

Janecky DR, Seyfried WE Jr. 1986. Hydrothermal serpentinization of peridotite within the oceanic crust: experimental investigations of mineralogy and major element chemistry. *Geochim. Cosmochim. Acta* 50:1357–78

Johannes W. 1969. An experimental investigation of the system MgO-SiO_2-H_2O-CO_2. *Am. J. Sci.* 267:1083–104

Kelemen PB, Kikawa E, Miller DJ, Natsue A, Bach W, et al. 2004. *Proceedings of the Ocean Drilling Program, Initial Reports*, Vol. 209. College Station, TX: Ocean Drill. Program

Kelemen PB, Kikawa E, Miller DJ, Party SS. 2007. Leg 209 summary: Processes in a 20-km-thick conductive boundary layer beneath the Mid-Atlantic Ridge, 14°–16°N. In *Proceedings of the Ocean Drilling Program, Scientific Results*, Vol. 209, ed. PB Kelemen, E Kikawa, DJ Miller, pp. 1–33. College Station, TX: Ocean Drill. Program

Kelemen PB, Matter JM. 2008. In situ carbonation of peridotite for CO_2 storage. *Proc. Natl. Acad. Sci. USA* 105:17295–300

Kelemen PB, Matter JM, Streit E. 2008. Field observations and theoretical studies relevant to enhanced in situ carbonation of peridotite. *Proc. Conf. Accel. Carbonation Environ. Mater. Eng., Oct. 1–3, Rome*, pp. 105–12. Rome: Sapienza Univ.

Kelley DS, Karson JA, Blackman DK, Früh-Green GL, Butterfield DA, et al. 2001. An off-axis hydrothermal vent field near the Mid-Atlantic Ridge at 30°N. *Nature* 412:145–49

Kelley DS, Karson JA, Früh-Green GL, Yoerger DR, Shank TM, et al. 2005. A serpentinite-hosted ecosystem: the Lost City hydrothermal field. *Science* 307:1428–34

Kerrick DM. 1974. Review of metamorphic mixed-volatile (H_2O-CO_2) equilibria. *Am. Mineral.* 59:729–62

Klein F, Bach W. 2009. Fe-Ni-Co-O-S phase relations in peridotite-seawater interactions. *J. Petrol.* 50:37–59

Klein F, Bach W, Jons N, McCollom T, Moskowitz B, Berquo T. 2009. Iron partitioning and hydrogen generation during serpentinization of abyssal peridotites from 15°N on the Mid-Atlantic Ridge. *Geochim. Cosmochim. Acta* 73:6868–93

Krevor SC, Graves CR, Van Gosen BS, McCafferty AE. 2009. Mapping the mineral resource base for mineral carbon-dioxide sequestration in the conterminous United States. *U.S. Geol. Surv. Digit. Data Ser. 414*. **http://pubs.usgs.gov/ds/414/**

Lackner KS, Wendt CH, Butt DP, Joyce EL, Sharp DH. 1995. Carbon dioxide disposal in carbonate minerals. *Energy* 20:1153–70

Lang SQ, Butterfield DA, Schulte MD, Kelley DS, Lilley MD. 2010. Elevated concentrations of formate, acetate and dissolved organic carbon found at the Lost City hydrothermal field. *Geochim. Cosmochim. Acta* 74:941–52

Launay J, Fontes J-C. 1985. Les sources thermales de Prony (Nouvelle-Calédonie) et leurs précipités chimiques: exemple de formation de brucite primaire. *Géol. Fr.* 1:83–100

Leblanc M, Ceuleneer G, Al Azri H, Jedwab J. 1991. Hydrothermal concentration of palladium and platinum in mantle peridotites from the Oman ophiolite. *C.R. Acad. Sci. Ser. II* 312:1007–12

Liteanu E, Spiers CJ. 2009. Influence of pore salt content on compaction creep of calcite aggregates in the presence of supercritical CO_2. *Chem. Geol.* 265:134–47

Lorand JP. 1987. A new occurrence of native iron in a serpentinized mantle peridotite—Maqsad, Sumail massif, Semail ophiolite (southern Oman). *C.R. Acad. Sci. Ser. II* 304:703–6

Lowell RP, Rona PA. 2002. Seafloor hydrothermal systems driven by the serpentinization of peridotite. *Geophys. Res. Lett.* 29(11):1531

Ludwig KA, Kelley DS, Butterfield DA, Nelson BK, Früh-Green G. 2006. Formation and evolution of carbonate chimneys at the Lost City hydrothermal field. *Geochim. Cosmochim. Acta* 70:3625–45

MacDonald AH, Fyfe WS. 1985. Rate of serpentinization in seafloor environments. *Tectonophysics* 116:123–35

Madu BE, Nesbitt BE, Muehlenbachs K. 1990. A mesothermal gold-stibnite-quartz vein occurrence in the Canadian Cordillera. *Econ. Geol.* 85:1260–68

Marini L. 2007. *Geological Sequestration of Carbon Dioxide: Thermodynamics, Kinetics, and Reaction Path Modeling*. Amsterdam: Elsevier. 470 pp.

Martin B, Fyfe WS. 1970. Some experimental and theoretical observations on kinetics of hydration reactions with particular reference to serpentinization. *Chem. Geol.* 6:185–202

Matter JM, Kelemen PB. 2009. Permanent CO_2 storage and mineral carbonation in geologic reservoirs. *Nat. Geosci.* 2:837–41

Matter JM, Waber HN, Loew S, Matter A. 2006. Recharge areas and geochemical evolution of groundwater in an alluvial aquifer system in the Sultanate of Oman. *Hydrogeol. J.* 14:203–24

Mazzotti M, Abanades JC, Allam R, Lackner KS, Meunier F, et al. 2005. Mineral carbonation and industrial uses of CO_2. In *IPCC Special Report on Carbon Dioxide Capture and Storage*, ed. B Metz, O Davidson, H de Coninck, M Loos, L Meyer, pp. 319–38. Cambridge: Cambridge Univ. Press

McCollom TM, Bach W. 2009. Thermodynamic constraints on hydrogen generation during serpentinization of ultramafic rocks. *Geochim. Cosmochim. Acta* 73:856–75

Milliken KL, Morgan JK. 1996. Chemical evidence for near-seafloor precipitation of calcite in serpentinites (Site 897) and serpentinite breccias (Site 899), Iberia abyssal plain. In *Proceedings of the Ocean Drilling Program, Scientific Results*, Vol. 149, ed. RB Whitmarsh, DS Sawyer, A Klaus, DG Masson, pp. 553–58. College Station, TX: Ocean Drill. Program

Milsch H, Seibt A, Spangenberg E. 2009. Long-term petrophysical investigations on geothermal reservoir rocks at simulated in situ conditions. *Transport Porous Media* 77:59–78

Morrow C, Moore D, Lockner D. 2001. Permeability reduction in granite under hydrothermal conditions. *J. Geophys. Res.* 106:30551–60

Mottl MJ, Komor SC, Fryer P, Moyer CL. 2003. Deep-slab fluids fuel extremophilic *Archaea* on a Mariana forearc serpentinite mud volcano: Ocean Drilling Program Leg 195. *Geochem. Geophys. Geosyst.* 4(11):9009

Mottl MJ, Wheat G, Fryer P, Gharib J, Martin JB. 2004. Chemistry of springs across the Mariana forearc shows progressive devolatilization of the subducting plate. *Geochim. Cosmochim. Acta* 68:4915–33

Nasir S, Al Sayigh AR, Al Harthy A, Al-Khirbash S, Al-Jaaidi O, et al. 2007. Mineralogical and geochemical characterization of listwaenite from the Semail ophiolite, Oman. *Chem. Erde Geochem.* 67:213–28

Neal C, Stanger G. 1983. Hydrogen generation from mantle source rocks in Oman. *Earth Planet. Sci. Lett.* 66:315–20

Neal C, Stanger G. 1984. Calcium and magnesium-hydroxide precipitation from alkaline groundwaters in Oman, and their significance to the process of serpentinization. *Mineral. Mag.* 48:237–41

Neal C, Stanger G. 1985. Past and present serpentinization of ultramafic rocks: an example from the Semail ophiolite nappe of northern Oman. In *The Chemistry of Weathering*, ed. JI Drever, pp. 249–75. Dordrecht, Neth.: D. Reidel

O'Connor WK, Dahlin DC, Rush GE, Gerdemann SJ, Nilsen DN. 2004. Aqueous mineral carbonation. *U.S. Dep. Energy Final Rep. DOE/ARC-TR-04-002*, U.S. Dep. Energy Albany Res. Cent., Albany

O'Hanley DS. 1992. Solution to the volume problem in serpentinization. *Geology* 20:705–8

O'Neil JR, Barnes I. 1971. ^{13}C and ^{18}O compositions in some fresh-water carbonates associated with ultramafic rocks and serpentinites: western United States. *Geochim. Cosmochim. Acta* 35:687–97

O'Neil JR, Clayton RN, Mayeda TK. 1969. Oxygen isotope fractionation in divalent metal carbonates. *J. Chem. Phys.* 51:5547–58

Palandri JL, Kharaka YK. 2004. A compilation of rate parameters of water-mineral interaction kinetics for application to geochemical modeling. *U.S. Geol. Surv. Open File Rep. 2004-1068*, U.S. Geol. Surv., Menlo Park, Calif.

Peretti A, Dubessy J, Mullis J, Frost BR, Tromsdorff V. 1992. Highly reducing conditions during Alpine metamorphism of the Malenco peridotite (Sondrio, northern Italy) indicated by mineral paragenesis and H_2 in fluid inclusions. *Contrib. Mineral. Petrol.* 112:329–40

Poupeau G, Saddiqi O, Michard A, Goffé B, Oberhänsli R. 1998. Late thermal evolution of the Oman Mountains subophiolitic windows: apatite fission-track thermochronology. *Geology* 26:1139–42

Pozzorini D, Früh-Green GL. 1996. Stable isotope systematics of the Ventina Ophicarbonate Zone, Bergell contact aureole. *Schweiz. Mineral. Petrogr. Mitt.* 76:549–64

Prigiobbe V, Costa G, Baciocchi R, Hänchen M, Mazzotti M. 2009. The effect of CO_2 and salinity on olivine dissolution kinetics at 120°C. *Chem. Eng. Sci.* 64:3510–15

Putnis A. 2009. Mineral replacement reactions. *Rev. Mineral. Geochem.* 70:87–124

Raupach MR, Marland G, Ciais P, Le Quéré C, Canadell JG, et al. 2007. Global and regional drivers of accelerating CO_2 emissions. *Proc. Natl. Acad. Sci. USA* 104:10288–93

Ribeiro Da Costa I, Barriga FJAS, Taylor RN. 2008. Late seafloor carbonate precipitation in serpentinites from the Rainbow and Saldanha sites (Mid-Atlantic Ridge). *Eur. J. Mineral.* 20:173–81

Robinson PT, Malpas J, Zhou MF, Ash C, Yang JS, Bai WJ. 2005. Geochemistry and origin of listwanites in the Sartohay and Luobnsa ophiolites, China. *Int. Geol. Rev.* 47:177–202

Royne A, Jamtveit B, Mathiesen J, Malthe-Sorenssen A. 2009. Controls on rock weathering rates by reaction-induced hierarchical fracturing. *Earth Planet. Sci. Lett.* 275:364–69

Rudge JF, Kelemen PB, Spiegelman M. 2010. A simple model of reaction-induced cracking applied to serpentinization and carbonation of peridotite. *Earth Planet. Sci. Lett.* 291:215–27

Saldi GD, Jordan G, Schott J, Oelkers EH. 2009. Magnesite growth rates as a function of temperature and saturation state. *Geochim. Cosmochim. Acta* 73:5646–57

Schaef HT, McGrail BP. 2009. Dissolution of Columbia River Basalt under mildly acidic conditions as a function of temperature: experimental results relevant to the geological sequestration of carbon dioxide. *Appl. Geochem.* 24:980–87

Schandl ES, Naldrett AJ. 1992. CO_2 metasomatism of serpentinites south of Timmins, Ontario. *Can. Mineral.* 30:93–108

Schandl ES, Wicks FJ. 1991. Carbonate and associated alteration of ultramafic and rhyolitic rocks at the Hemingway Property, Kidd Creek Volcanic Complex, Timmins, Ontario. *Econ. Geol.* 88:1615–35

Scherer GW. 1999. Crystallization in pores. *Cement Concrete Res.* 29:1347–58

Scherer GW. 2004. Stress from crystallization of salt. *Cement Concrete Res.* 34:1613–24

Schrag D. 2007. Preparing to capture carbon. *Science* 315:812–13

Schramm B, Devey C, Gillis KM, Lackschewitz K. 2005. Quantitative assessment of chemical and mineralogical changes due to progressive low-temperature alteration of East Pacific Rise basalts from 0 to 9 Ma. *Chem. Geol.* 218:281–313

Schuiling RD. 1964. Serpentinization as a possible cause of high heat-flow values in and near the oceanic ridges. *Nature* 201:807–8

Schuiling RD. 2006. Mineral sequestration of CO_2 and recovery of the heat of reaction. In *Macro-Engineering: A Challenge for the Future*, ed. V Badescu, RB Cathcart, RD Schuiling, pp. 21–29. Dordrecht, Neth.: Springer

Schuiling RD, Krijgsman P. 2006. Enhanced weathering: an effective and cheap tool to sequester CO_2. *Clim. Change* 74:349–54

Seifritz W. 1990. CO_2 disposal by means of silicates. *Nature* 345:486

Seyfried WE Jr, Foustoukos DI, Fu Q. 2007. Redox evolution and mass transfer during serpentinization: an experimental and theoretical study at 200°C, 500 bar with implications for ultramafic-hosted hydrothermal systems at Mid-Ocean Ridges. *Geochim. Cosmochim. Acta* 71:3872–86

Shervais JW, Kolesar P, Andreasen K. 2005. A field and chemical study of serpentinization, Stonyford, California: chemical flux and mass balance. *Int. Geol. Rev.* 47:1–23

Skippen G. 1974. An experimental model for low pressure metamorphism of siliceous dolomitic marble. *Am. J. Sci.* 274:487–509

Smith JR, Giegengack R, Schwarcz HP. 2004. Constraints on Pleistocene pluvial climates through stable-isotope analysis of fossil-spring tufas and associated gastropods, Kharga Oasis, Egypt. *Palaeogeogr. Palaeoclimatol. Palaeoecol.* 206:157–75

Snow JE, Dick HJB. 1995. Pervasive magnesium loss by marine weathering of peridotite. *Geochim. Cosmochim. Acta* 59:4219–35

Spiers CJ, Schutjes TM, Brzesowsky RH, Peach CJ, Liezenberg JL, Zwart HJ. 1990. Experimental determination of constitutive parameters governing creep of rocksalt by pressure solution. *Geol. Soc. Lond. Spec. Publ.* 54:215–27

Stanger G. 1985. Silicified serpentinite in the Semail nappe of Oman. *Lithos* 18:13–22

Stanger G. 1986. *The Hydrogeology of the Oman Mountains*. Durham, UK: The Open Univ.

Stanger G, Laver J, Neal C. 1988. Black carbonaceous calcite associated with serpentinite from Oman. *Mineral. Mag.* 52:403–8

Stanger G, Neal C. 1994. The occurrence and chemistry of huntite from Oman. *Chem. Geol.* 112:247–54

Staudigel H, Hart SR. 1985. Dating of ocean crust hydrothermal alteration: strontium isotope ratios from Hole 504B carbonates and a reinterpretation of Sr isotope data from Deep Sea Drilling Project Sites 105, 332, 417, and 418. *Deep Sea Drill. Proj. Initial Rep.* 83:297–303

Steiger M. 2005a. Crystal growth in porous materials: I. The crystallization pressure of large crystals. *J. Cryst. Growth* 282:455–69

Steiger M. 2005b. Crystal growth in porous materials: II. Influence of crystal size on the crystallization pressure. *J. Cryst. Growth* 282:470–81

Tarutani T, Clayton RN, Mayeda TK. 1969. The effect of polymorphism and magnesium substitution on oxygen isotope fractionation between calcium carbonates and water. *Geochim. Cosmochim. Acta* 33:987–96

Tenthorey E, Scholz CH, Aharonov E, Léger A. 1998. Precipitation sealing and diagenesis: 1. Experimental results. *J. Geophys. Res.* 103:23951–67

Trommsdorff V, Evans BW. 1977a. Antigorite-ophicarbonates: phase relations in a portion of the system $CaO\text{-}MgO\text{-}SiO_2\text{-}H_2O\text{-}CO_2$. *Contrib. Mineral. Petrol.* 60:39–56

Trommsdorff V, Evans BW. 1977b. Antigorite-ophicarbonates: contact metamorphism in Valmalenco, Italy. *Contrib. Mineral. Petrol.* 62:301–12

Vasconcelos C, McKenzie JA, Warthmann R, Bernasconi SM. 2005. Calibration of the $\delta^{18}O$ paleothermometer for dolomite precipitated in microbial cultures and natural environments. *Geology* 33:317–20

Walder J, Hallet B. 1985. A theoretical model of the fracture of rock during freezing. *Geol. Soc. Am. Bull.* 96:336–46

Weyhenmeyer CE. 2000. *Origin and evolution of groundwater in the alluvial aquifer of the eastern Batinah coastal plain, Sultanate of Oman: a hydrogeochemical approach*. PhD thesis. Univ. Bern, Switz. 202 pp.

Weyhenmeyer CE, Burns SJ, Waber HN, Macumber PG, Matter A. 2002. Isotope study of moisture sources, recharge areas, and groundwater flow paths within the eastern Batinah coastal plain, Sultanate of Oman. *Water Resour. Res.* 38:1184

Wilde A, Simpson L, Hanna S. 2002. Preliminary study of Cenozoic alteration and platinum deposition in the Oman ophiolite. *J. Virtual Explor.* 6:7–13

Wilson SA, Dipple GM, Power IM, Thom JM, Anderson RG, et al. 2009. Carbon dioxide fixation within mine wastes of ultramafic-hosted ore deposits: examples from the Clinton Creek and Cassiar chrysotile deposits, Canada. *Econ. Geol.* 104:95–112

Xu WY, Apps JA, Pruess K. 2004. Numerical simulation of CO_2 disposal by mineral trapping in deep aquifers. *Appl. Geochem.* 19:917–36

Annual Review
of Earth and
Planetary Sciences
Volume 39, 2011

Contents

Indexes

Errata

An online log of corrections to *Annual Review of Earth and Planetary Sciences* articles may be found at http://earth.annualreviews.org